Polymer Chemistry

Multi-stimuli responsive tetra-PPO_{60}-PEO_{20} ethylene diamine block copolymer enables pH, temperature, and solvent regulation of Au nanoparticle composite plasmonic response

Journal:	*Polymer Chemistry*
Manuscript ID	PY-ART-07-2019-001098.R2
Article Type:	Paper
Date Submitted by the Author:	30-Oct-2019
Complete List of Authors:	Diouf, Sokjna; Los Alamos National Laboratory Williams, Darrick; Los Alamos National Laboratory Seifert, Sönke; Argonne National Laboratory Londono-Calderon, Alejandra; Los Alamos National Laboratory Pettes, Michael; Los Alamos National Laboratory, Center for Integrated Nanotechnologies, Materials Physics and Applications Sheehan, Chris; Los Alamos National Laboratory Firestone, Millicent; Los Alamos National Laboratory

Multi-stimuli responsive tetra-PPO_{60}-PEO_{20} ethylene diamine block copolymer enables pH, temperature, and solvent regulation of Au nanoparticle composite plasmonic response

[1]Sokhna I-Y. F Diouf, [1]Darrick J. Williams, [2]Sönke Seifert, [1] Alejandra Londoño-Calderon, [1]Michael T. Pettes, [1]Christopher J. Sheehan, and [1]Millicent A. Firestone*

[1]Los Alamos National Laboratory, Los Alamos, NM USA 87545
[2]Argonne National Laboratory, Lemont, IL USA 60439

(*) Author to whom correspondence should be addressed:
Millicent A. Firestone
Materials Physics & Applications
Center for Integrated Nanotechnologies
Los Alamos National Laboratory
P.O. Box 1663

Los Alamos, NM 87545
Phone: 505-695-8837
E-mail: firestone@lanl.gov

Abstract

A gold nanoparticle (NP) hydrogel composite prepared by multi-step cascade synthesis undergoes temperature, pH, and solvent dependent nanoscale structural transformations promoting modulation of the plasmon resonance. The composite is spontaneously prepared from a non-covalent lamellar structured lyotropic mesophase (complex fluid) composed of amphiphiles (DMPC and Triton X-100) that support the reactive constituents, a mixture of hydroxyl and acrylate end-derivatized Tetronic (Poloxamine) polymer and $[AuCl_4]^-$. The reaction sequence begins with the reduction of $[AuCl_4]^-$ by the ethylene diamine linkage and PEO blocks of the Tetronic, yielding Au NP. The redox reaction generates free radicals initiating crosslinking of the acrylate end-derivatized polymer producing a chemical hydrogel. Optical spectroscopy and STEM confirm Au NP formation. ATR/FT-IR spectroscopy and thermal analysis establish acrylate crosslinking and network formation. X-ray scattering reveals the composite reversibly converts between multilamellar and bicontinuous cubic structures as temperature is increased above 35 °C for composites containing protonated ethylene diamine linkages (un-buffered water or acidic buffer). The reversible changes in nanoarchitecture red shifts and broadens the collective plasmon (from 523 nm to 575 nm) of the composite, an observation attributed to re-organization of confined NPs from 2D sheets (lamellae) to 1D columns (bicontinuous cubic channels). Composites prepared in alkaline buffer do not undergo a structural conversion with temperature, retaining a multilamellar architecture. In addition to pH and thermo-responsivity, the composite swells reversibly in polar solvents, which acts to de-aggregate and aggregate the encapsulated nanoparticles and varies the plasmon resonance by Δ52 nm. This work reports the first combined use of a polymer to achieve both the *in-situ* synthesis of spatially confined plasmonic NPs and their reversible stimuli-triggered re-organization mediated by interconvertible changes in scaffold nanoarchitecture.

Keywords: cascade synthesis, multi-stimuli-responsive, scaffold-mediated organization, plasmon tuning, gold nanoparticles

Introduction

Tremendous effort has been directed towards the creation of materials to harvest the remarkable intrinsic properties of inorganic nanoparticles (NPs).[1] Much of the effort on the synthesis of inorganic nanoparticle (NP) polymer composites has chiefly focused on approaches to collect NPs within an unstructured matrix, seeking to stabilize the NPs and preserve their individual properties.[2,3] There is growing interest in the preparation of structured polymeric scaffolds that control NP dispersion state thereby improving properties for technological applications[4], to produce new phenomena or to create multi-functional materials.[2,5-7] By far, the most thoroughly studied area in NP fillers has been their use for improving polymer mechanical properties.[8] The addition of NPs to ion conducting polymers have been shown to enhance directional ion transport.[9] Emergent electrical conductivity has been imparted to a nanostructured polymerized ionic liquid through scaffold-mediated columniation of Au NPs.[10,11] In parallel with quiescent NP assembly, investigators have sought ways to actively control NP organization for functional modulation of composites.[2] Stimuli-responsive NP polymer composites are important for advancing a wide range of technological applications. For example, magnetic (Fe_3O_4) NPs have been used to manipulate elastic polymers for shape defined actuation in soft robotics.[12] Surface-enhanced Raman Spectroscopy based sensors relying on creation of so-called “hot spots” between plasmonic (Au, Ag) NPs and have benefited from being embedded in thermo-responsive polymers that reversibly de-aggregate the NPs to promote analyte uptake and tightly repack them for optimized sensing.[13]

Typically, dynamic change in NP assemblies has been achieved through exploitation of stimuli-driven expansion/contraction of the supporting matrix to yield aggregation / de-aggregation

of the NPs.[14] This approach has been demonstrated through, for example, exploitation of thermally sensitive hydrogen bonding interactions between NP ligands and the polymer matrix.[15] Alternatively, a thermoresponsive polymer such as poly(*N*-isopropylacrylamide) has proven useful for reversible aggegration.[16] DNA constructs have also been extensively studied for thermoresponsive and pH modulation of NP arrangement.[17] Another approach involves solvent swelling of polymer hydrogels to reversibly control NP aggregation states.[18] More recently, gas absorption has been shown to trigger changes in polymer volume and is used to regulate NP aggregation.[19,20] For example, protonation of the tertiary amine groups in polymer single chain particles (SCPs) composed of polystyrene-*b*-poly(*N,N*—dimethylaminoethylmethacrylate)-*co*-4-methyl-[7-(methylacryloyl)oxy-ethyl-oxy]coumarin upon CO_2 exposure drives a volume increase in aqueous solution causing de-aggregation of encapsulated Au NPs. Contraction of the polymer is achieved by N_2 purging thereby producing a 'breathing" type dynamic modulation of the polymer scaffolding. While many examples of NP polymer composites that reversibly interconvert between disordered NP aggregates to de-aggregated states exist, surprisingly little work advancing dynamic regulation of NP spatial arrangement has been reported.[17] A path forward for achieving such a NP polymer composite would involve the use of interconvertible nanostructured polymers that confine and spatially organized encapsulated NPs. In other words, exploit stimuli-responsive polymers to mediate a transformation in NP ordering via scaffold structural changes. For example, reversible switching between multidimensional (2D layers) organization to 1D columniation of NPs to yield a tunable photonic and/or electronic composite. The work reported herein seeks to address this opportunity by exploiting the stimuli-responsive properties of chemically crosslinked polymer networks for the reversible dimensional organization of metal (Au) plasmonic NPs leading

to tunable plasmonic response (color tuning).

Previously, we reported the use of nanostructured complex fluids, mixtures of molecular and macromolecular amphiphiles dispersed in water as scaffolding for the spatial organization of metal NPs.[21] Complex fluids offer an attractive approach for the preparation of nanostructured composites given their compositional flexibility, which allows for enhancing guest (NP) compatibility and directing the region of NP localization. In addition, the individual amphiphiles can be easily replaced or chemically modified to tune the self-assembled structure and/or adjust physical properties (e.g., viscoelasticity). Given that complex fluids are non-covalent self-assembled materials they are, however, unable to withstand certain environmental conditions (e.g., dissolution upon exposure to organic solvents) and are mechanically fragile (i.e., not self-supporting). Chemical crosslinking of self-assembled non-covalent systems affords an approach to stabilize the complex fluids to yield durable multicompartmental materials (i.e., segregated hydrophilic water regions and hydrophobic alkane domains).[22,23] The *in-situ* synthesis of Au NPs concurrent with chemical crosslinking of the complex fluid has been demonstrated through the adaptation of the principles of cascade synthesis.[24] Briefly, introduction of a metal salt ($[AuCl_4]^-$) into the aqueous phase of the self-assembled complex fluid containing a diacrylated non-ionic PEO_{117}-PPO_{47}-PEO_{117} triblock macro-monomer (Pluronic F98), lipid (DMPC) and zwitterionic amine *N*-oxide co-surfactant (LDAO) spontaneously generated Au NPs. The gold redox chemistry during NP formation produces free radicals that in turn initiate the chemical crosslinking of the acrylate moieties leading to the generation of a monolithic Au NP nanostructured chemical gel composite.[24] The Au NP polymer hydrogel composite reversibly swells in water. The solvent induced volume expansion promotes de-aggregation of the *in-situ* synthesized Au NPs causing

observable and reversible changes in the collective plasmonic response of the composite. Here, we seek to go beyond simple stimuli-responsive NP aggregation – de-aggregation through the introduction of an additional stimuli-responsive characteristic which triggers dimensional changes in the supporting hydrogel matrix. This is accomplished by replacing the linear triblock copolymer with a tetra-arm copolymer, PEO_{60}-PPO_{20}, Tetronic 1107 (Poloxamine), possessing a central ethylenediamine core to introduce pH and thermoresponsivity to the solvent responsive composite. The diamine core imparts the added benefit of allowing for replacement of the amine-*N*-oxide (LDAO) co-surfactant, needed for gold reduction and NP formation. Thus, a broader range of co-surfactants (here for example, a non-ionic co-surfactant, Triton X-100) serving to expand complex fluid compositions. [25]

Experimental

Materials and Methods. Tetronic 1107 (Ethylenediamine tetrakis(propoxylate-*b*-ethoxylate) tetrol) was obtained from BASF Corporation (Mount Olive, NJ). Lyophilized dimyristoyl-*sn*-glycero-3-phosphocholine, DMPC (> 99%) was purchased from Avanti Polar Lipids (Alabaster, AL). Triton-X 100 (laboratory grade) and Hydrogen tetrachloroaurate (III), $HAuCl_4$ (99.9 %) was purchased from Sigma-Aldrich (Milwaukee, WI). Potassium phosphate dibasic (98 %) and monobasic (99 %), sodium acetate (≥ 99.0 %), and glacial acetic acid (≥ 99.7 %) were purchased from Fisher Scientific (Pittsburgh, PA). Diethyl ether (≥ 99.0 %), Acryloyl Chloride (98.0 %), Dichloromethane (≥ 99.5 %), Potassium carbonate (> 99 %) was obtained from VWR (Denver, CO). All chemicals were used as received. Milli-Q (18 MΩ·cm) water was used for sample preparation.

Tetronic 1107 tetraacrylate (2). Tetronic 1107 (*1*) was used as received. Tetronic 1107 (2.0 g, 0.066 mmol) was dissolved in anhydrous dichloromethane (32 mL) at room temperature followed by the addition of K_2CO_3 (0.900 g, 6.9 mmol). Distilled acryloyl chloride (0.39 mL, 0.7 mmol) was added dropwise over a 2-5 min timeframe. The reaction mixture was stirred for 12 h at room temperature. Potassium carbonate was removed from the reaction mixture by filtration through Cellite™ (Ward Hill, MA) supported on a glass frit. The Tet1107$(Acr)_4$ solution was reduced under vacuum at 35 ^oC to yield a viscous liquid. The product was precipitated with Et_2O (60 mL), filtered, and dried under vacuum to remove the volatile impurities. The extent of polymer functionalization was determined by ^1H NMR spectroscopy. Briefly, ^1H NMR spectrum integration was normalized to the number of methyl protons (δ 1.14 ppm) of the PPO block (20 x 3 x 4 = 240). A ratio of the actual integration value (derived from the recorded spectrum) for the acrylate protons (6.43, 6.16,

5.83 ppm) in the aromatic region over the expected value for the functionalized polymer provides an estimation of the percent functionalization (Fig. S1). ^{1}H NMR (500 MHz, $CDCl_3$) δ: 6.44 (d, J = 17.3 Hz), 6.17 (dd, J = 9.23, Hz), 5.85 (d, J = 10.4 Hz), 4.32 (t, J = 4.8 Hz), 3.79-3.42 (m). ATR/FT-IR: 1725 cm^{-1} (vC=O), 2882 cm^{-1} diprotonated EDA-linkage (vCH_2), 2862 cm^{-1} neutral EDA-linkage (vCH_2).

Preparation of Tetronic 1107(Acr)$_4$ based complex fluid. A quaternary composition consisting of Φ_s = 0.0371 ± 0.0005 Triton-X 100 co-surfactant (Fig. 1A (i)), and Φ_L = 0.0858 ± 0.0005 DMPC lipid (Fig. 1A, (ii)), Φ_p = 0.147 ± 0.0005 Tetronic 1107(Acr)$_4$ (Fig. 1A, (iii)) was prepared by hydration of the solid components in 0.733 ± 0.001 weight fraction (Φ_w) of water. This was accomplished by repeated cycles of heating (45-50 ^{o}C), vortex mixing, and cooling in an ice bath until a macroscopic optically uniform sample is formed. Complex fluids prepared in buffered aqueous solution employed 0.1 M sodium acetate pH 3.66, or 0.01 M sodium carbonate buffer pH 9.02.

Cascade synthesis of Au NP crosslinked hydrogel. To a pre-formed Tetronic1107(Acr)$_4$ – based complex fluid (see above), $[AuCl_4]^-$, is added to achieve a concentration of 6.5±0.6 mM (20 µL of a 135±5 mM $[AuCl_4]^-$ aqueous solution into 0.5 mL complex fluid). Addition of the Au^{3+} initiates the cascade synthesis. The sample is heated at 50 °C until cessation of color changes and a solid material is produced.

Photopolymerization of Tetronic1107(Acr)$_4$ based complex fluid. The complex fluid is loaded into a borosilicate Pasteur pipet then photo irradiated with a high-intensity UV light source (Hanovia 400 W

mercury arc lamp, λ ~ 254 nm) for 2 h. The resulting solid was removed from the pipet by breaking with a razor blade, washed in water, yielding a pale yellow, elastic, self-supporting solid.

Physical Methods. ^{1}H NMR spectroscopy was performed on a Bruker model DMX 500 NMR spectrometer (11.7T) equipped with a three-channel, 5-mm inverse detection, three-axis gradient, and variable temperature probe with ^{2}H lock at 76.773 MHz. The temperature was maintained at 295 K by the use of nitrogen pre-cooler, heater coil, and the variable temperature controller. ATR / FT-IR spectroscopy was performed using a Thermo Scientific spectrometer over the wavenumber range 4000-400 cm^{-1} with spectra recorded at 4 cm^{-1} resolution and averaged over 256 scans. Thermogravimetric analysis (TGA) was carried out on a TA Instrument Q500 by heating a known amount of sample (1-5 mg) in a platinum pan from 20 ^{o}C, to a final temperature of 500 ^{o}C, at a rate of 5 ^{o}C/min under N_2 flow. Differential scanning calorimetry (DSC) was performed using a TA instruments Q2000 (New Castle, DE) with a refrigerated cooling system, purged with N_2 at 2 ^{o}C min^{-1}. Calibration was performed using an indium standard. Sample (2 – 6 mg) were sealed in aluminum pans and equilibrated at −60 °C prior to scanning. Data was collected over two heating- cooling cycles with a temperature range of -60 °C – 100 °C. UV/Visible spectroscopy was collected using a Shimadzu UV2600 spectrophotometer (Kyoto, Japan) operating in single beam configuration over the wavelength region 200 - 900 nm. Temperature control was achieved using a Peltier element (Shimadzu TCC-100 Thermoelectrically Controlled Cell holder) inserted in the spectrophotometer. Bulk composites were studied in transmission mode as thin slices, created using a razor blade, derived from the bulk material. Diffuse reflectance spectroscopy on a bulk sample (Fig. S12) was to used confirm the validity of

transmission UV-Vis spectroscopy. Diffuse reflectance measurements were made using a DT-1000 CD UV-Vis light source equipped with SD2000 charge-coupled (CCD) detector under OOI Base32 software (Ocean Optics, Dunedin, FL).

Scanning Transmission Electron Microscope (STEM) analysis was carried out on released NPs dropwise deposited on ultra-thin carbon TEM grids. Briefly, the well-entrained NPs are released from the polymer matrix by disrupting the crosslinks through treatment with an aqueous solution of hydrazine. Typically, 40 mg Au NP polymer composite is swollen in 2 mL of water for 2 h, followed by the addition of 1 mL of a 37 (V/V) % aqueous solution of hydrazine. After 7 days, the solid material dissolved, leaving a magenta colored solution. These samples were imaged using an insertable detector in a FEI Magellan 400 XHR-SEM. The sample was imaged at 30 kV in bright-field mode. Image analysis was carried out using ImageJ (NIH, Bethesda, MD), an open source software. Direct imaging of gird cast Au NP polymer composites (i.e., cascade reaction on the carbon film TEM grid type-B (Ted Pella, Inc.) were imaged using an image corrected FEI Titan 80-300 kV microscope at the LANL Electron Microscopy Laboratory operating at 80 kV. High-angle annular dark field S/TEM (HAADF-STEM) images of the composite were collected at 80 kV using a camera length of 100 mm and a C2 aperture of 70 μm.

Small- and wide-angle X-ray scattering (SWAXS) measurements were performed using the pin-hole setups at the undulator beamline 12ID at the Advanced Photon Source (APS) at Argonne National Laboratory (Lemont, IL). Data collected at station C (12 / 18 keV) used either a custom-built CCD detector composed of 4 CCD chips and features a 180 mm square active area with 1024 x 1024 pixel resolution or a MARCCD detector composed of 9 CCD chips featuring 300 mm square active area with 2048 x 2048 pixel resolutions. The sample-to-detector distance

provided a *q*-range from 0.006 – 0.6 $Å^{-1}$ or 0.005 – 0.7 $Å^{-1}$. Data collected at station B simultaneously collected both SAXS and WAXS data used both a Pilatus 2M detector for SAXS and a Pilatus 300K for WAXS. For all measurements, the scattering vector, *q*, was calibrated with silver behenate employing the characteristic diffraction ring at q = 0.1076 $Å^{-1}$. The collected scattering images were averaged to produce plots of scattering X-ray intensity, I(*q*), versus the scattering vector, *q*, where $q=4\pi\sin(\theta) / \lambda$. Liquid phase samples were held in 1.5 mm quartz capillaries. Durable, self-supporting polymers were supported on a custom-built holder. The averaged scattering patterns were background subtracted using data collected on buffers held in 1.5 mm quartz capillaries or air for the liquid and solid phase samples respectively. Temperature control was achieved using a custom-built Peltier holder.

Results and Discussion

In this report we examine the use of a multi-stimuli-responsive tetra-acrylated block copolymer, tetra-PPO_{20}-PEO_{60}, Tetronic 1107 (Poloxamine) (*1*) as a reactive macro-monomer for the cascade synthesis of a gold nanoparticle (Au NP) crosslinked complex fluid composite. The acrylate end-derivatized tetra-PPO_{20}-PEO_{60} block copolymer, henceforth referred to as Tet1107$(Acr)_4$,(*2*), was synthesized by adapting a previously reported procedure for the acrylation of PEO_{117}-PPO_{47}-PEO_{117} triblock copolymer.[24] In brief, the acrylation is achieved by esterification of the terminal hydroxyl groups of the Tet1107 (*1*) PEO blocks with acryloyl chloride in the presence of base, potassium carbonate (Scheme 1). The purified product is isolated by precipitation in diethyl ether. ^{1}H NMR spectroscopy confirms macro-monomer formation by the appearance of the acrylic proton resonance located at 6.44, 6.17, 5.85 ppm (Fig. S1). The degree of acrylation typically achieved is between 90 - 95 % based upon comparison of the sum of the acrylic proton integration values to the expected twelve acrylate protons, normalized to the methyl protons from the PPO blocks (3 x 4(60) = 720) (Fig. S1). Successful acrylation is further corroborated by ATR/FT-IR spectroscopy (Fig. S2) through the existence of the acrylate signature mode at 1725 cm^{-1} (C=O stretching) and the loss of the OH vibrational mode at 3462 cm^{-1}.[24] The nature of the ethylene diamine linkage (i.e., neutral, mono-protonated, di-protonated) is determined by examination of the ethylene linkage CH_2 modes.[26] Specifically, a neutral ethylene diamine CH_2 mode is expected in the region 2861-2866 cm^{-1}. A mono-protonated and/or a di-protonated linkage positioned at 2872 cm^{-1}, 2882 cm^{-1}, respectively. Both the Tet1107 and the Tet1107$(Acr)_4$ ethylene CH_2 modes are found at 2882 cm^{-1} and 2862 cm^{-1}, indicating the presences of a mixture of di-protonated and neutral states (Fig. S2).

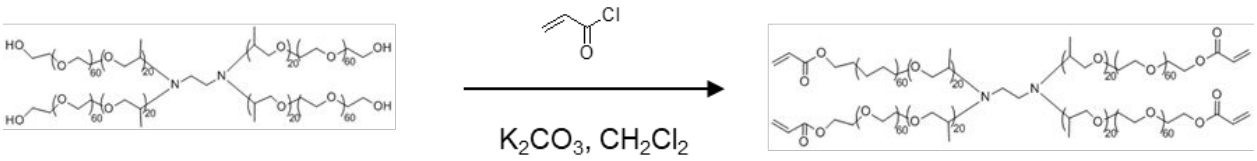

(*1*) (*2*)

Scheme 1. Acrylation of Tet1107 (*1*) to yield Tet1107(Acr)$_4$, (*2*)

Composite synthesis. The freshly synthesized tetra-acrylated block copolymer is used in the preparation of the Au NP crosslinked complex fluid, by first preparing a non-reactive complex fluid that lacks the $[AuCl_4]^-$. The non-reactive complex fluid contains the tetra-acrylated block copolymer, (Poloxamine), tetra-PPO_{20}-PEO_{60}, Tet1107(Acr)$_4$ (Fig. 1, iii), a saturated phospholipid, dimyristoyl-*sn*-glycero-3-phosphocholine, DMPC (Fig. 1, ii), and a non-ionic co-surfactant, Triton X-100 (Fig. 1, i) in aqueous (here, un-buffered) solution, and forms a macroscopically uniform, optical transparent mixture (Fig. 2A,i) at room temperature. The non-reactive complex fluid reversibly converts between a viscous-liquid at room temperature to an optically opaque fluid upon heating (to 50 °C). Cooling the complex fluid on ice (~ 3 °C) transitions the sample to a physical gel. Addition of $[AuCl_4]^-$, to achieve a concentration of 6.5±0.6 μM, imparts a pale-yellow color and initiates the cascade reaction (Fig. 2A, ii). After brief incubation at 50 °C (~9 min) the complex fluid color intensifies to bright yellow (Fig. 2A, iii). The continued heating (50 °C) of the mixture (~22 min) produces a purple color (Fig. 2A, iv) which transitions to a very dark burgundy color after ~ 42 min of continued heating (Fig. 2A, v). The distinct color changes are consistent with reduction of Au^{3+} to Au^0 and formation of Au NPs.[24] Eventually (~ 30-45 min) the sample

becomes a waxy solid that is easily removed from the vial and retains the shape of the vial in which it is prepared (Fig. 2A, vi). Optical spectra, recorded at select times during composite formation (Fig. S3A) affirm a blue shift and narrowing of the extinction peak (absorption + scattering) during reaction progression. The loss of fluidity and conversion into a mechanically durable solid implies chemical crosslinking of the terminally appended acrylate groups on the tetra-PEO-PPO block copolymer. The observed sequence of color changes (yellow to red) and the production of a solid suggests the gold redox chemistry yields sufficient free radicals to initiate acrylate crosslinking, a cascade reaction sequence similar to that previously proposed for the DMPC/F98$(Acr)_2$/LDAO complex fluid derived Au NP polymer composite (Fig. 2C).[24]

The role of Tet1107$(Acr)_4$ as the reactive macro-monomer for both Au NP formation and chemical crosslinking is exemplified by monitoring color changes and product outcome upon substitution with F98$(Acr)_2$, a linear triblock copolymer lacking the central diamine linkage in the complex fluid formulation, prepared with the non-ionic co-surfactant, Triton X-100. As clearly evident in Fig. 2B, the observed color transitions recorded after $[AuCl_4]^-$ addition are notably different than observed for compositions containing Tet1107$(Acr)_4$. That is, the pale-yellow color transitions to a rose-pink color, denoting reduction of Au^{3+} to Au^0 and NP formation (Fig. 2Bii to iii). Although the complex fluid color continues to intensify (pale purple to burgundy) upon further incubation at 50 ^oC (21 h, Fig. 2B iv, v), the sample never attains sufficient mechanical durability to become a self-supporting solid (144 h at 50 ^oC, Fig. 2B vi). Monitoring the optical spectrum at periodic intervals during the reaction reveals rapid emergence of a broad extinction peak at ~ 550 nm (between 2-14 min.). As the reaction continues only a minor blue shift and insignificant narrowing is observed of the extinction peak is observed (Fig. S3B). The breadth of the peak

suggests large Au NP aggregates that do not evolve in time. Another observed difference in the cascade reaction progression between the previously reported system, employing the DMPC/F98$(Acr)_2$/LDAO/H_2O-based complex fluid, and the current formulations (DMPC/Tet1107$(Acr)_4$/Triton X-100/H_2O) and (DMPC/F98$(Acr)_2$/Triton X-100/H_2O) is the noted absence of the transient blue color phase during gold reduction.[24] Spectroscopically it was determined the blue phase possessed a very broad extinction peak that spanned a spectral range 480 nm to 1100 nm (centered ~ 790 nm) signaling the formation of very large (highly poly-disperse) NP agglomerates.[24] It was hypothesized that agglomeration arose from weakened PEO association of rapidly generated Au NPs. The temporal dissipation of the blue phase and transition to a red-purple color indicated de-agglomeration driven by an oxidative etching process acting to morphological re-shape the Au NPs. Collectively these findings suggest, unlike the Tet$(Acr)_4$ composition, replacement with F98$(Acr)_2$ in the current formulation appears to inhibit oxidative etching, serving to alter the production of free radicals leading to limited acrylate crosslinking. Differences are further revealed using a standard DPPH, diphenylpicryl-hydrazyl, a free radical scavenger colorimetric assay to monitor free radical activity (Fig S4). The assay confirms differences in free radical kinetics between the Tet$(Acr)_4$ and F98$(Acr)_2$ compositions with slow sustained production in the former compared to the later. Thus, the diamine linkage is deemed important for achieving both Au NP formation and initiation of acrylate crosslinking. This finding is further supported by the previously reported cascade synthesis which employed a complex fluid formulation (DMPC/F98$(Acr)_2$/LDAO/H_2O) containing the co-surfactant LDAO, a zwitterionic amine-*N*-oxide also functions as a co-reducing agent with PEO. Thus, an amine co-reducing agent appears to be important for sustaining efficient redox chemistry during the cascade

synthesis.[27] The replacement of F98(Acr)$_2$ with Tet117(Acr)$_2$ allows for formulation of complex fluids using a wide range of co-surfactants, not just amines.

Chemical gel characterization. Successful crosslinking of the macro-monomer and formation of a chemical (polymer network) gel is further verified, in part, by vibrational spectroscopy (Fig. 3). The spectrum shows a strong vibrational mode at 1734 cm^{-1} confirming production of unconjugated acryloyl carbonyls (C=O stretching).[24] Vibrational modes characteristic of the phospholipid are also observed including the symmetric and asymmetric alkyl methylene carbon vibrational modes at 2917 cm^{-1} and 2850 cm^{-1}.[24] The position of the $\nu(CH_2)_{sym}$ and $\nu(CH_2)_{asym}$ modes indicate the lipid alkyl chains are well-ordered, adopting predominately an all-trans conformation state.[28] The symmetric and asymmetric PO_2^- stretching modes are found at 1090 cm^{-1} and 1203 cm^{-1}, respectively.[29] Additional lipid modes are located at 825 cm^{-1} (ν(–C-N$^+$-(CH$_3$)$_3$ headgroup) and 719 cm^{-1} ($\rho(CH_2)$ head + chains).[30] Collectively, these vibrational signatures provide evidence that the lipid is retained during polymerization and after post polymerization washing. The nature of the PEO/PPO blocks from the Tetronic, and to a lesser extent the oligomeric EO unit of Triton X-100 within the composite is evaluated through comparison of the IR spectra collected on the Au-NP composite to the Tet1107 (Fig. 3B *vs*. Fig. S2, blue curve). Both spectra show expected modes at 1467 cm^{-1} (CH_2 bending), 1102 cm^{-1} (C-O-C stretch) from Tetronic and Triton X-100.[24 31] Modes uniquely found in the Au NP composite, but not observed in the pure Tet1107 spectrum, include 1326 cm^{-1} (crystalline PEO CH_2 wagging & C-C stretch), 1257 cm^{-1} (crystalline PEO CH_2 twist), and 928 cm^{-1} (PEO metal salt) all signal high crystalline PEO content is induced during *in-situ* Au NP production.[24] This finding is supported by the work of others, which has shown addition of

metal salt to an aqueous solution of Pluronics induces a greater degree of PEO segment crystallinity.[32] In addition to the ethylene oxide modes, Triton X-100 is confirmed by the aromatic ring modes positioned at 1489 cm^{-1} and 1507 cm^{-1} (coupling of aromatic ring C-C stretching and C-H deformation modes).[33,34] Modes providing information on the state of the Tetronic diamine linkage is gleaned from comparison of the composite (Fig. 3A) and the polymer only spectra (Fig. S2A). Once again the protonation state of the ethylene diamine linkage is evaluated through the CH_2 modes of the ethylene linkage.[35] In the Au NP composite a single peak is found at 2873 cm^{-1} indicating the Tetronic ethylene diamine linkage is solely in the mono-protonated state in unbuffered water. Lastly, the low frequency region of the composite IR spectrum provides an indication of gold ethylenediamine association through the appearance of several modes uniquely identified in the composite at 449 cm^{-1}, 463 cm^{-1}, 470 cm^{-1}, and 519 cm^{-1}, all have been previously reported and associated with metal-nitrogen stretching frequencies.[36] Thus, IR spectroscopy finds the Au NPs are positioned/ stabilized by the protonated ethylene diamine nitrogen and the ethylene oxide of the PEO moieties.

The thermal characteristics of an air-dried Au NP composite are investigated by thermogravimetric analysis (TGA). The TGA carried out using fast scan (5 °C min^{-1}) studies under N_2 display a complex decomposition profile before reaching 400°C, consistent with the decomposition of the various starting materials and products formed in the Au NP composite (Fig. 4A). The first region of weight loss, up to 150°C, reflects removal of water from the composite (region *i*). The loss of water (2.7 wt. % from 73.3 wt. %) within the composite compared to the "as prepared" starting complex fluid prior to reaction initiation indicates significant dehydration during crosslinking and Au NP formation. After loss of solvent, the next region of thermal decomposition

(*ii*) occurs at 255.3°C. An identical transition was observed for the linear triblock PEO_{117}-PPO_{47}-PEO_{117} ($F98(Acr)_2$) derived Au NP composite and attributed to crosslinking-induced acrylate bond scission.[37] The third event (*iii*), located at 287.3°C signals the thermal evaporation / decomposition of the Triton X-100 co-surfactant.[38] The fourth component at 332.2°C is ascribed to the decomposition of DMPC (*iv*).[29] The fifth and largest decomposition step occurs at 388.2°C (*v*) and is due to the thermal decomposition of $Tet1107(Acr)_4$. The position of this loss compares well with that previously determined for $F98(Acr)_2$.[24] Finally a small decomposition event absent in the photocrosslinked network lacking Au NPs (Fig. S5A) is noted at 533.7 °C (0.65 wt. %) and may reflect crosslinked Tetronic – Au NP nodes. That is the increased thermal decomposition of PEO/ Au NPs has been previously observed and attributed to enhanced thermal stability from association / proximity to the NPs.[39] The residual mass (4.7 wt. %) provides an indication of the Au NP content within the composite.

The DSC heating and cooling scans collected on the Au NP composite (Fig. 4B) possess the expected order-disorder transition (crystalline to amorphous/molten PEO state) at 53.6°C.[24] The ability of EO chains to pack and form crystalline regions in a crosslinked network have been noted and can occur during dehydration of the polymer.[40] The location of the thermal transition compares well to that previously determined for Au NP composites prepared with $F98(Acr)_2$ (53.5°C).[24] Here, however, a second larger peak is also observed at 39.5°C. The thermogram is similar to that recorded on the polymerized complex fluid lacking Au NPs (Fig. S5B) which also displays two melting transitions at the same locations but with the majority component occurring at the lower temperature (37.8°C). The work of others has shown that the melting points of PEO can vary significantly from that of neat PEO homopolymer. For example, PEO melting was found

to decrease by 8 – 9°C in blends.[41] PEO homopolymer confined within cylindrical nanopores observed a 10°C drop in T_m.[41] A greater decrease in PEO melting temperature (T_m - 27.3°C to 55.3°C) was found for diblock copolymers of polystyrene-*b*-poly(ethylene oxide) and attributed to a decrease in PEO segmental mobility.[42] Thus, the appearance of two distinct phase transitions may arise from the temperature-induced structural phase transition which acts to vary PEO confinement (see below).

Assessment of Au NPs. As noted, the appearance of a deep burgundy color indicates $[AuCl_4]^-$ to Au^0 reduction and formation of plasmonic Au NPs. The optical spectrum recorded on a dehydrated composite (Fig. 5A, left) displays a broad surface plasmon resonance (SPR) maximum at 545 nm (Fig. 5B, black curve). The expected position for isolated, well-dispersed spherical Au NPs in the size range 3-20 nm is expected at ca. 527 nm.[24] Thus, the red-shifted SPR suggests matrix-assisted NP aggregation (i.e., inter-particle coupling). The broad SPR reflects several populations of the Au NPs adopting a variety of close packed arrangements.

Scanning transmission electron microscopy (STEM) provides direct confirmation and assessment of the particle morphology. A representative STEM image collected on particles released from a water swollen chemical gel treated with an aqueous solution (37 (v/v) %) of hydrazine and deposited on a Cu TEM grid shows a large collection of spherical particles, and to a lesser extent a population of triangular plate-like particles (Fig. S6A). The average spherical particle diameter was determined to be 9.4 nm and are highly polydisperse, ranging from 4 - 22 nm (Fig. S6B). Additional STEM experiments performed directly on thin films formed on Cu TEM grids by cascade synthesis confirm the release experiments. The STEM performed directly on

contracted, de-swollen composites (under vacuum) reveal collections of linear chains and rafts of Au NPs (Fig. S6C-F). These are particle arrangements we would predict being favored given the internal template structure of the complex fluid.

Complex fluid nanostructure. Changes in PEO block stabilization of the forming Au NPs and/or coordination with the ethylene diamine linkage of Tetronic may be facilitated by differences between Tet1107(Acr)$_4$ *vs* F98(Acr)$_2$ macro-monomer association or partitioning into the supporting lipid bilayer. Evaluation of the temperature-dependent SAXS profiles on the pre-reactive complex fluid prepared in water (pH 6.8, a value between the pka$_1$ and pka$_2$ of Tet1107) can provide insight into Tet1107(Acr)$_4$ association with the DMPC bilayer. The temperature-dependent SAXS data collected on the self-assembled pre-reactive complex fluid formulation, that is a complex fluid lacking the $[AuCl_4]^-$, is presented in Fig. 6A. At 20°C (Fig. 6A, blue curve) a broad correlation peak, centered at ~ $q = 0.12_6$ Å^{-1}, is observed possibly indicating formation of a weakly ordered non-lamellar phase. A similar scattering profile has been reported for complex fluid compositions prepared with the polymer component introduced as a lipid conjugate (PEG5000-DMPE) at reduced temperatures (5°C).[43] Complementary small-angle neutron scattering (SANS), a technique that provides greater scattering contrast between aqueous and organic phases, proved the existence of a 2-D hexagonal array of prolate micelles.[44] Here, in addition to the non-lamellar phase, the presence of a small component of a lamellar phase is noted by two low intensity peaks riding on top of the broad peak (q = 0.097 and 0.19 Å^{-1}). At 30°C, the SAXS profile (Fig. 6A, black curve) is dominated by two sharp diffraction peaks positioned at $q = 0.10_6$ (001) and 0.21_2 (002) Å^{-1}. The integral order spacing signals conversion to a multi-

lamellar mesophase having an inter-lamellar, *d*-spacing, of 59 Å. The scattering curve compares favorably with that previously reported for a simple DMPC (30 wt. %) aqueous dispersion (q = 0.099 and 0.19_8 Å^{-1}; *d*-spacing = 63 Å) and complex fluids prepared employing the weak bilayer associating linear triblock copolymers, such as, F68, PEO_{75}-PPO_{30}-PEO_{75}.[43] At 40 ^{o}C, a low q small amplitude correlation peak emerges at q = 0.048 Å^{-1} with retention of the lamellar diffraction signatures (Fig. 6A, orange curve). The broad low q peak heralds the emergence of crystalline EO chains, produced by dehydration, contained within the inter-lamellar water channels.[24] The feature ascribed to crystalline EO sharpens (q = 0.047 Å^{-1}) upon increasing the temperature to 50^{o}C (Fig. 6A, red curve). Further noted is the co-existence of two lamellar phases. An expanded multi-lamellar phase (the minority component) with a lattice dimension, *d*-spacing of 104 Å (q = 0.060_4 (001), 0.12_1 (002), 0.18_5 (003) Å^{-1}) and a contracted multi-lamellar structure (a majority component), *d*-spacing of 61 Å (q= 0.10_3 (001), 0.20_5 (002) Å^{-1}). The appearance of an expanded multi-lamellar structure signals a fraction of the Tet1117 adopts a configuration within the supporting lipid/Triton X-100 bilayer to facilitate projection the PEO blocks perpendicular from the bilayer (Fig. 6B). The vertically projected PEO generates steric pressure between opposing bilayers, causing expansion (swelling) of the interstitial water layer.[44,45] Thus, replacement of the linear triblock copolymer F98 with Tet1117 results in the collapsed (smaller lattice spacing) multilamellar structure being favored over the expanded lamellar architecture. This finding is consistent with the hindered transmembrane insertion of the protonated form of Tet1117 within the bilayer (Fig. 6B, right).[24]

As reported for the PEO_n-PPO_m-PEO_n linear triblock copolymer-based complex fluids, here too the self-assembled Tetr1107-based complex fluid structure depends on the number of

repeat units in the hydrophobic PPO blocks.[43,46] Prior SAXS studies showed linear triblock copolymers possessing short hydrophobic propylene oxide (PO) chain lengths, those of molecular repeats of 15 and 30 (F38 and F68) with a radius of gyration, R_g (assuming a Gaussian chain) between 7 - 12 Å did not have sufficient length to span the alkane portion of a DMPC bilayer, estimated to be ca. 20 Å.[43,46] The X-shaped 4 arm Tet1107 contains 20 molecular repeat units in the PPO blocks giving an R_g of ca. 10 Å. The coupling of the PPO blocks through the central ethylenediamine linkage, however, effectively doubles the number of repeat units (to 40 Å) and R_g (~ 20 Å) making the molecular length sufficient for transmembrane insertion into the hydrophobic portion of a DMPC bilayer (Fig. 6B, left). In addition to satisfying the requirement of adequate molecular length of the hydrophobic PPO units, the hydrophobicity of the ethylenediamine core, determined by the degree of protonation, is an additional factor that must be considered. Although Poloxamines are generally considered non-ionic surfactants, the central diamine group can be neutral, mono-protonated, or di-protonated depending on the pH. The di-protonated form predominates at pH values less than 4 (pka_1 is in the range of 4.0 - 5.6).[47] The mono-protonated form is found at a pH range between pka_1 and pka_2 (pka_2 is in the range of 7.5 - 8.1).[47] Above pH 8 the diamine linkage is neutral rendering the PPO-diamine segment hydrophobic, a state most compatible with full immersion into the alkyl chain region of the bilayer (Figure 6B, left). Below pH 8, however, the amine moiety is converted to an ammonium group, the core becomes hydrophilic, acting to reposition the Tet1117 within the bilayer. Specifically, the protonated form of Tetronic would reside closer to the polar lipid headgroup region of the bilayer. The shallow insertion, stabilized by electrostatic interaction between the diamine core linkage and the DMPC headgroup, could cause the polymer to adopt a “staple-like” configuration (Fig. 6B,

right).[48]

Given that association of Tet1117 with the supporting bilayer is dependent on the degree of protonation of the ethylene diamine linkage, the structure of complex fluids prepared in acid and alkaline buffer were examined. Temperature-dependent SAXS patterns collected on complex fluid compositions prepared in acetate buffer (pH 3.66) retains a collapsed lamellar structure at 20 °C (*d*-spacing of 63 Å), as evidenced by the two diffraction peaks located at $q = 0.10_0$ (001), 0.19_8 (002) Å^{-1} (Fig. S7A). Elevation of temperature (to 40 °C and 50 °C) the expanded lamellar phase (*d*-spacing = 116 Å) dominates the scattering pattern (q = 0.053 (001), 0.11_0 (002), 0.16_5 (003), 0.20_3 (004) Å^{-1}). A reduction in structural coherence of the lamellar phases at all temperatures is observed as evidenced by the increased width of the diffraction peaks, in comparison to samples prepared in water (Fig. 6A *vs.* S7A). Thus, increased protonation of the Tetronic ethylene diamine linkage causes increased disruption of the supporting bilayer and stabilizes the expanded lamellar structure.

In alkaline buffer (10 mM carbonate buffer, pH 9.02), a condition which increases the Tet1117 neutral ethylene diamine linkage content (Fig. S7B). The scattering profile looks very similar to that recorded for complex fluids prepared in unbuffered water, possessing a broad correlation peak at q ~0.13 Å^{-1}, signaling a weakly ordered non-lamellar phase, at 25 °C (Fig. S5B, blue curve). At 40 °C, a contracted multi-lamellar phase with a *d*-spacing of 63 Å dominates the scattering pattern (Fig. S7B, orange curve). A small secondary lamellar component having an expanded *d*-spacing of 101.8 Å is also found. In the low q-region a small amplitude correlation peak at q = 0.044 Å^{-1} confirms crystalline EO (Fig. S7B, orange curve). At 50 °C (Fig. S7B, red curve), an increase in the expanded multilamellar phase at the expense of the contracted lamellar

phase, as verified by the increased amplitude of the Bragg reflections positioned at $q = 0.066_7$ (001), 0.13_2 (002) $Å^{-1}$. The expanded lamellar structure interlayer spacing is the same as for samples prepared in un-buffered water but less than that found for those made with acidic buffer. Thus, complex fluids prepared in alkaline buffer self-assemble into a mixture of both expanded and contracted multilamellar nanostructures at elevated temperatures possessing lattice dimensions similar to that of complex fluids prepared in un-buffered water. Unlike samples prepared near neutral pH, alkaline conditions favor enrichment of the expanded lamellar phase possibly due to the neutral diamine linkage of Tet1107 favoring transmembrane insertion.

Au NP composite nanostructure. The Au NP composite structure was determined by using a combination of both small- and wide-angle X-ray scattering, SAXS/WAXS (Fig. 7A, B, respectively). The SAXS profile collected on the as-synthesized composite, derived from a mesophase prepared in un-buffered water, at 22°C (Fig. 7A) shows a pattern featuring five sharp diffraction peaks at $q = 0.11_5$ (001), 0.23_1 (002), 0.34_6 (003), 0.46_1 (004), 0.69_3 (006) $Å^{-1}$ consistent with formation of a well-ordered multilamellar structure having a repeat distance, $d = 55$ Å. The diffraction pattern compares well to that collected on a composition prepared by UV-initiated free radical polymerization but lacking $[AuCl_4]^-$ (Fig. 7C). The no gold containing crosslinked hydrogel SAXS profile has diffraction peaks at $q = 0.12_0$ (001), 0.23_7 (002), 0.36_2 (003), 0.47_8 (004) $Å^{-1}$ and a lattice spacing, d, of 52 Å. The observed minor reduction in the lattice dimensions compare to the composite most likely arises from water content variation (i.e., differences in sample dehydration). Interestingly, both the no gold and gold containing crosslinked hydrogels do not adopt an expanded lamellar structure as was found for mesophases above room temperature.

Further noted, is both the composite and no gold polymer composite scattering patterns include broad, small amplitude features in the low *q*-region. The low *q* feature in the polymer only sample is centered at ~ 0.041 $Å^{-1}$ (153 Å). The Au NP-polymer composite contains a broader correlation peak in the low *q* region centered ~ at 0.046 $Å^{-1}$ (137 Å). The low *q* scattering components are attributed to crystallized EO chains confined within the inter-lamellar water channels.[49] More specifically, arising from metastable crystalline states of non-integrally folded (NIF) EO chains of varying folding length.[49] Under the strong confinement imposed by the short lamellar repeat distance, the crystalline EO stems orient parallel to the membrane surface. The role of confinement (weak *vs.* strong) on regulating the orientation of crystalline EO chains has been recently discussed in clay composites.[50] The presence of crystalline EO for the Au NP polymer composite is further supported by the WAXS pattern collected on the Au-polymer composite (Fig. 7B). The WAXS pattern shows diffraction peaks at q = 1.36 (4.6 Å) and 1.65 $Å^{-1}$ (3.8 Å), confirming the crystalline EO.[51] The sharp peak at q = 1.50 $Å^{-1}$ (4.17 Å) in the wide-angle pattern (Fig. 7B) is assigned to the ordered amphiphilic hydrocarbon chains within the alkyl bilayer (i.e., phospholipids). The chain-chain correlation distance of 4.17 Å is consistent with the supporting amphiphile bilayer adopting an untilted L_β phase. Collectively, the X-ray scattering data indicates the composite is a collapsed multilamellar structure with Au NPs confined within the semi-crystalline PEO chains localized in the compressed inter-lamellar water layers. The determined structure compares well to that previously reported for Au NP F98-based composites synthesized via a cascade approach.[24]

Thermoresponsivity. Temperature-dependent x-ray scattering profiles collected on the Au NP composite is shown in Fig. 8. At reduced temperature, 15°C (Fig. 8, blue curve), the multilamellar structure observed at room temperature is retained (Fig. 7A). Fours integral orders of diffraction are observed at q = 0.11_6 (001), 0.23_1 (002), 0.34_8 (003), 0.46_4 (004) $Å^{-1}$ with an intra-lamellar spacing of d = 55 Å. Very little variation in the scattering pattern is found upon increasing the temperature to 20°C (Fig. 8, black curve). Further increasing the temperature to 35°C, however, causes notable changes in the SAXS pattern (Fig. 8C, orange curve; Table S1). The diffraction peaks of a remnant lamellar phase are found at q = 0.12_6 (001), 0.25_4 (002), 0.38_2 (003), 0.51 (004) $Å^{-1}$ with a d-spacing of 50 Å. In addition, a set of 12 Bragg reflections are located at q = 0.11_6 (110), 0.16_4 (200), 0.20_0 (211), 0.23_1 (220), 0.25_4 (310), 0.28_4 (222), 0.30_7 (321), 0.33_2 (400), 0.34_7 (411), 0.38_2 (332), 0.41_0 (431), 0.46_8 (440) $Å^{-1}$, (√2, √4, √6, √8, √10, √12, √14, √16, √18, √22, √26, √23) indexing to a cubic structure with a lattice parameter of 77 Å (Table S1). The low relative intensity of the 211 and 200 peaks coupled with the relative peak positions points toward a cubic Im3m (Q^{229}) structure. The Im3m cubic phase is a primitive inverse bicontinuous phase sometimes referred to as the "plumber's nightmare" structure (Fig. 8, 35 °C, inset).[52] The phase consists of two unconnected water channels separated by the amphiphile bilayer. The lattice is composed of six tubular struts with nodes at 90 ° angles. This structure is a minimal surface morphology in which the interfacial area between the two volumes (here, aqueous and organic, alkyl chains) is minimized. Prior work reported that Tetronics can induce remodeling of the lipid bilayer. For example, at reduced temperature SAXS studies carried out on Tet1107 aqueous dispersions have been found to form spherical micelles at 30 wt. %. The unimers reorganize into a FCC or 2D hex micellar structures with increasing temperature.[53] The phase change is believed

to be driven by the decreasing water solubility of the Tetronic PPO block[53]. Lamellar-to-cubic phase transitions in phospholipid bilayer systems incorporating linear nonionic triblock copolymers PEO-PPO-PEO (P85) have also been observed.[54] The observed temperature-driven reversible conversion from lamellar to cubic may also be ascribed to increasing lipid chain splay induced by the polymer (i.e., amphiphile molecular geometry transitioning from cylindrical to wedge shape or conical).[55] [56] Studies on lipids have shown phase changes are often due to subtle variations in molecular shape. The lipid monoolein, for example, upon addition of certain detergents, salts, sugars, proteins, DNA triggers alkyl chain splay generating a lipid of conical molecular shape and producing cubic phase structures.[57] Thus, it is possible that with increasing temperature, and therefore decreasing water solubility of the PPO/PEO blocks of the Tetronic polymer, induces sufficient hydrocarbon splay to transform the composite to a cubic phase.

The influence of the temperature driven lamellar-to-cubic structure change on the collective optical properties of the encapsulated Au NPs was evaluated by Vis-NIR spectroscopy (Fig. 9). At 25°C, when the composite structure is a well-ordered multi-lamellar phase the SPR is centered at ~ 523 nm (Fig. 9A, green curve). Upon heating the composite to 35°C, and conversion to the cubic Im3m structure, the SPR red shifts to 540 nm along with increased extinction spanning ~ 650 – 800 nm (Fig. 9A, orange curve). The red shifting of the SPR with increasing temperature suggests matrix-assisted changes in the NP packing arrangement (i.e., closer inter-particle coupling). The broadening of the SPR reflects several populations of the Au NPs adopting a distribution of close-packed arrangements. Further noted is the decrease in the amplitude of the SPR, from increased opacity at elevated temperatures. At 55°C the SPR continues to red shift (to 576 nm), broaden, and diminish in intensity (Fig. 9A, red curve). The observed changes in the Au

NP composite optical characteristics are fully reversible as demonstrated by monitoring the Vis-NIR spectra upon cooling to 20°C (Figure 9B). The observed reversible changes in optical spectra track with temperature driven changes in matrix nanostructure. The matrix assisted SPR modulation is further supported by monitoring the Vis-NIR of Au NP composites prepared with the corresponding F98$(Acr)_2$ and F68$(Acr)_2$/LDAO/DMPC based complex fluids (Fig. S8). As previously reported, both compositions do not undergo a thermally driven structural transformation to a non-lamellar cubic phase and the temperature-dependent SPR of the Au NP composites are found to slightly red shift from 527 nm to 534 nm with increasing temperature (10°C to 50°C). The observed minor change in SPR with increasing temperature here are due to increased water insolubility and contraction of the PEO blocks (driven by decreasing water solubility at elevated temperatures), serves to compress NP organization.

Solvent responsivity. The Tetronic derived Au NP composite reversibly swells in water (Fig. 5A). The equilibrium swelling ratio was determined according to the following, $r = m_t/m_0$, where m_0 is the mass of

the dry network and m_t the mass at time interval t during swelling in water. The maximum equilibrium mass-swelling ratio is attained within 24 h and found to be 6.8. The swelling ratio is slightly greater than that determined for the Au NP F98$(Acr)_2$/DMPC/LDAO based composite (r= 5.1).[24] No detectable loss of the Au NPs was found after extended exposure (swelling) to water. Thus, the Au NPs are well entrained within the matrix (as stated earlier the Au NPs could only be released from the matrix through hydrazine digestion of the crosslinked network). Structural evolution of the water induced swollen crosslinked complex fluid was monitored by SAXS (Fig.

7D). The scattering profile for the water swollen gel shows a broad feature approximately located at q = 0.16 Å^{-1}. After 33 min of de-swelling in air, considerably sharper (more intense) diffraction peaks emerge (q = 0.11, 0.22, 0.32, 0.44 Å^{-1}) signifying re-establishment of the well-ordered multi-lamellar structure (d-spacing 57 Å). With continued air-drying (t = 43 min), a slight shifting of the diffraction peaks to higher q, consistent with loss of water is observed. At 52 min, a broad feature (correlation peak) in the low q region (0.065 Å^{-1}) emerges signaling formation of crystalized PEO.

The influence of swelling and de-swelling on the optical properties of the Au NP composite are similarly evaluated by Vis-NIR spectroscopy (Fig. 5B). In the contracted, dehydrated state, the composite SPR maximum is 545 nm. Conversely, in the water-swollen state the SPR narrows and blue shifts with a peak maximum at 527 nm. This reversible switching between non-interacting (de-aggregated) Au NPs (527 nm) in a disordered water swollen lamellar structure to a red-shifted SPR in the contracted de-swollen lamellar state is comparable to that reported previously for the F98(Acr)$_2$ /LDAO /DMPC-complex fluid derived composite.[24]

pH responsivity. Temperature-dependent changes in nanostructure can also be correlated to the extent of protonation of the ethylene diamine linkage. As discussed, composites prepared in un-buffered water (pH 6.8), contain an ethylene diamine linkage primarily in the mono-protonated form leads to a reversible structural transition from multi-lamellar to cubic with increasing temperature (Fig. 8). Temperature-dependent SAXS studies performed on composites prepared employing an acidic buffer (100 mM sodium acetate, pH 3.6), which produces a mixture of di- and mono-protonated ethylene diamine, experiences a similar lamellar to cubic phase transition (Fig. S9). The conversion, however, occurs at a slightly elevated temperature (at 45°C *vs.* 35°C)

compared to the materials prepared in un-buffered water. The lamellar to cubic structural transformation gives rise to similar temperature-driven changes in the plasmon resonance of the composites (Fig. S10B). Specifically, below the phase transition (T < 45°C) the SPR is centered at ~ 522 nm. Conversely, the SPR red shifts to ~ 540 nm and broadens, consistent with confinement in the 1D channel structure of the bicontinuous cubic architectures.

The temperature-dependent X-ray scattering collected on composites prepared in alkaline buffer (10 mM potassium carbonate, pH 9) did not exhibit the lamellar to cubic structural conversion (Fig. S11), but retains a multi-lamellar structure over the entire temperature range examined (10°C to 80°C). The lack of a cubic phase is consistent with the greater neutral character of the ethylene diamine linkage under basic conditions as predicted promotes transmembrane insertion of the Tetronic in the supporting amphiphile bilayer. The transmembrane configured polymer does not lead to lipid chain splay and hence the driving force to generate a cubic structural transformation is lacking. The inability to structural transform the matrix does not produce any detectable changes in the temperature-dependent SPR (Fig. S10C). That is the SPR remains centered at 518 nm consistent with the Au NPs being organized in a non-interacting fashion confined within the 2D sheet-like architecture provided by the lamellar structure.

Conclusions

The work reported herein presents a scalable, versatile strategy that combines the principles of cascade reaction chemistry with bottom-up self-assembly to synthesize a multi-stimuli-responsive plasmonic NP hydrogel composite. The composite is robust yet re-configurable allowing for dimensional re-organization of the *in-situ* synthesized NPs within the nanostructured scaffold. The use of a tetrablock block copolymer, tetra-PPO_{20}-PEO_{60}, Tet1107 (Poloxamine), supported within a lipid / co-surfactant bilayer, serves a critical role in the execution of two consecutive reaction steps (gold reduction followed by free-radical initiated crosslinking of acrylate) to produce the composite. The polymer also imparts pH and temperature responsivity to the formed nanostructured composite. The Au NP composite undergoes a thermo-reversible nanostructure transformation from multi-lamellar to a bicontinuous cubic phase, as determined by SAXS, when the ethylene diamine linkage is protonated (i.e., prepared using un-buffered water, pH 6.8 and/or under acidic conditions, pH 3.6). The structural transformation between a multi-lamellar to bicontinuous nanostructure is uniquely achieved through the intercalation of the polymer within the supporting lipid / co-surfactant bilayer. This observation is in contrast to prior work on Au NP Tetronic micelles, where the surface coated Au NP – polymer micelles undergo a simple hydration – dehydration expansion and contraction.[58] Furthermore, unlike the work reported herein where the *in-situ* synthesized Au NPs, confined in the hydrophilic region of the hydrogel matrix are coordinated by PEO and the ethylene diamine moiety of the Tet1107 as revealed by vibrational spectroscopy and thermal analysis. The temperature-driven change in scaffolding architecture promotes spatial reconfiguration of the NPs as evidenced by the red shift

of the plasmon resonance upon conversion into a bicontinuous cubic structure that contains 1D aqueous channels. Composites prepared in water, at temperatures below 35°C, adopt a multi-lamellar structure and display a SPR of 527 nm, signaling well dispersed, non-interacting spherical Au NPs. The non-aggregated Au NPs are attributed to confinement within 2-dimensional aqueous layers of the multi-lamellar structure. Conversely, the composite SPR red shifts to 576 nm and broadens, consistent with increased particle-particle interactions upon conversion to the inverted bicontinuous primitive cubic architecture (Im3m). The bicontinuous primitive cubic structure contains channel-like water regions that act to direct 1-dimensional columnar organization of the confined Au NP thereby promoting greater interaction (aggregation). It is anticipated that increasing the Au NP number packing density within the matrix could further red shift the SPR and/or create a percolated 1D network of NPs producing emergent electrical conductivity. Composites prepared under acidic conditions exhibit similar behavior. Conversely, samples prepared with alkaline buffer, used to reduce the amount of protonated ethylene diamine linkage of the Tetronic to not exhibit temperature-driven structural transformations, remaining lamellar over a wide temperature range. The absence of a structural transition suppresses temperature induced modulation of the Au NP internal packing as reflected in the lack of detectable change in the SPR.

Furthermore, the use of the Tetronic block copolymer offers greater versatility in the formation of reactive complex fluids, thereby broadening the range of co-surfactants (i.e., to include non-amines) usable in the self-assembled complex fluid formulation. The stable reconstitution of functional membrane proteins (e.g., photosynthetic reaction center) will be enabled through expansion in the range of co-surfactants useable in the complex fluid

formulation.[59] Thus, the synthetic principles and dynamic nanostructured hydrogel reported herein may prove useful for the fabrication of functional abiotic (inorganic NP) – biotic (protein) composites. Preliminary studies exploring both complex fluids compositions suitable for cascade synthesis of Ag and Pt NP polymer composites have also been carried out and will provide a path forward for expanding the utility of cascade synthesized metal NP polymer composites. The ability to both prepare a wide range of NP polymer composites and co-integrate functional biomolecules will allow for adapting these materials to a range of nanobiotechnology applications, including, for example, SPR- or SERS-based biosensing, and/or implantable antimicrobial surgical dressing.[3]

Acknowledgements

The authors thank Dr. Bryan Ringstrand for assistance in optimizing Tetronic acrylation. This work was performed, in part, at the Center for Integrated Nanotechnologies (CINT). CINT is funded through the DOE Office of Basic Energy Sciences. Los Alamos National Laboratory is operated by Triad National Security LLC for the National Nuclear Security Administration of U.S. Department of Energy (Contract No. 89233218CNA000001). This research used resources at the Advanced Photon Source, a U.S. Department of Energy (DOE) Office of Science User Facility operated for the DOE Office of Science by Argonne National Laboratory under Contract No. DE-AC02-06CH11357.

Figure Captions

Figure 1. Molecular structure (left panel) and schematic representation (right panel) of constituents used in the preparation of Au NP Tetronic-based composites. (i) Triton X-100; (ii) dimyristoylphosphatidycholine, DMPC); (iii) Tet117$(Acr)_4$.

Figure 2. (A) Selected photographs collected during the spontaneous formation of Au NPs and crosslinking using a Tet117$(Acr)_4$/DMPC/Triton X-100/H_2O based complex fluid. (i) Complex fluid prior to addition of $[AuCl_4]^-$ is a low viscosity liquid at room temperature. (ii) Addition of $[AuCl_4]^-$ the complex is pale yellow and becomes a bright yellow after 9 min at 50 ^oC, (iii). (iv) At 22 min of incubation at 50 ^oC, the sample becomes a light purple physical gel. (v) After 42 min of incubation at 50 ^oC, the complex transitions to a burgundy physical gel. (vi) Further heating does not cause further color changes but after ~ 30-45 min the physical gel becomes a durable, self-supporting chemical gel that takes on the shape of the vial in which it is prepared. (B) Selected photographs collected during the spontaneous formation of Au NPs using a F98$(Acr)_2$/DMPC/Triton X-100/H_2O-based complex fluid (i) as it spontaneously progresses from an initial pale-yellow mixture (ii); light taupe mixture (iii); to a rose taupe mixture (iv); to lilac mixture (v). The mixture never solidified into a self-supporting chemical gel (vi). (C) Proposed cascade reaction scheme for the formation of the Au NP Tetronic composite.

Figure 3. High frequency (A) and low frequency (B) ATR/FT-IR spectra recorded on the Au NP composite prepared in un-buffered water.

Figure 4. (A) Fast scan (5 $^oC\ min^{-1}$) TGA collected on the Au NP composite, under N_2 atmosphere, weight % (black) and derivative weight loss, (blue). (B) DSC heating and cooling scans (2 $^oC\ min^{-1}$) collected on Au NP composite prepared in un-buffered water.

Figure 5. (A) Photograph of contracted (de-swollen) and swollen Au NP composite in water, (B) Vis-NIR of water swollen (red curve) and de-swollen in air (black curve).

Figure 6. Temperature-dependent SAXS profiles collected at 20 °C, 30 °C, 40 °C, 50 °C on a complex fluid mesophase, prior to addition of $[AuCl_4]^-$. (B) Schematic illustration of proposed Tetronic configurations within the supporting bilayer. Neutral Tet117$(Acr)_4$ transmembrane inserting into a DMPC/Triton X-100 bilayer (left). Protonated Tet117$(Acr)_4$ residing in a single leaflet of a DMPC/Triton X-100 bilayer (right).

Figure 7. Representative (A) SAXS and (B) WAXS circularly averaged data collected on the Au NP composite at 21 °C (sample prepared with un-buffered water). (C) SAXS profile collected on a polymer prepared by photo-initiated free radical polymerization. (D) Time evolution of SAXS pattern collected during dehydration under ambient conditions of a fully water swollen composite.

Figure 8. Temperature dependent SAXS profiles collected on the Au NP composite prepared in un-buffered water. Patterns collected at 15 °C and 20 °C are lamellar structured (schematic shown as inset on 15 °C). Patterns collected at 35 °C and 55 °C are cubic (schematic shown as inset on 35 °C).

Figure 9. UV-Vis-NIR spectra collected on the Au NP composite prepared in un-buffered water. (A) Spectra recorded heating from room temperature to 55 °C then cooled to 10 °C. (B) Spectra recorded cooling from 50 °C.

TOC. Dynamic plasmonic tuning of Au NP organization through pH and temperature mediated polymer architecture transformation from lamellar to bicontinuous cubic structures

References

(1) Grzelczak, M.; Vermant, J.; Furst, E. M.; Liz-Marzán, L. M. Directed Self-Assembly of Nanoparticles. *ACS Nano* **2010,** *4* (7), 3591.

(2) Firestone, M. A.; Hayden, S. C.; Huber, D. L. Greater than the sum: Synergy and emergent properties in nanoparticle-polymer composites. *Mrs Bull* **2015,** *40* (9), 760.

(3) Thoniyot, P.; Tan, M. J.; Karim, A. A.; Young, D. J.; Loh, X. J. Nanoparticle-Hydrogel Composites: Concept, Design, and Applications of These Promising, Multi-Functional Materials. *Adv Sci* **2015,** *2* (1-2).

(4) Kumar, S. K.; Benicewicz, B. C.; Vaia, R. A.; Winey, K. I. 50th Anniversary Perspective: Are Polymer Nanocomposites Practical for Applications? *Macromolecules* **2017,** *50* (3), 714.

(5) Zhang, J.; Santos, P. J.; Gabrys, P. A.; Lee, S.; Liu, C.; Macfarlane, R. J. Self-Assembling Nanocomposite Tectons. *J Am Chem Soc* **2016,** *138* (50), 16228.

(6) Genix, A.-C.; Oberdisse, J. Nanoparticle self-assembly: from interactions in suspension to polymer nanocomposites. *Soft Matter* **2018,** *14* (25), 5161.

(7) Kao, J.; Thorkelsson, K.; Bai, P.; Rancatore, B. J.; Xu, T. Toward functional nanocomposites: taking the best of nanoparticles, polymers, and small molecules. *Chem Soc Rev* **2013,** *42* (7), 2654.

(8) Elmelegy, T.; El-Tayeb, N. s. M. *Synergistic Effect of Different Nanoparticles Hybridization on Mechanical Properties of Epoxy Composite*, 2014.

(9) Cheng, S.; Smith, D. M.; Pan, Q.; Wang, S.; Li, C. Y. Anisotropic ion transport in nanostructured solid polymer electrolytes. *Rsc Adv* **2015,** *5* (60), 48793.

(10) Lee, S.; Cummins, M. D.; Willing, G. A.; Firestone, M. A. Conductivity of ionic liquid-derived polymers with internal gold nanoparticle conduits. *J Mater Chem* **2009,** *19* (43), 8092.

(11) Lee, S.; Ringstrand, B. S.; Stone, D. A.; Firestone, M. A. Electrochemical Activity of Glucose Oxidase on a Poly(ionic liquid)-Au Nanoparticle Composite. *Acs Appl Mater Inter* **2012,** *4* (5), 2311.

(12) Liu, J. A.-C.; Gillen, J. H.; Mishra, S. R.; Evans, B. A.; Tracy, J. B. Photothermally and magnetically controlled reconfiguration of polymer composites for soft robotics. *Science Advances* **2019,** *5* (8), eaaw2897.

(13) Strozyk, M. S.; de Aberasturi, D. J.; Liz-Marzan, L. M. Composite Polymer Colloids for SERS-Based Applications. *Chem Rec* **2018,** *18* (7-8), 807.

(14) Tokarev, I.; Minko, S. Tunable plasmonic nanostructures from noble metal nanoparticles and stimuli-responsive polymers. *Soft Matter* **2012,** *8* (22), 5980.

(15) Heo, K.; Miesch, C.; Emrick, T.; Hayward, R. C. Thermally Reversible Aggregation of Gold Nanoparticles in Polymer Nanocomposites through Hydrogen Bonding. *Nano Lett* **2013,** *13* (11), 5297.

(16) Han, F.; Soeriyadi, A. H.; Vivekchand, S. R. C.; Gooding, J. J. Simple Method for Tuning the Optical Properties of Thermoresponsive Plasmonic Nanogels. *ACS Macro Letters* **2016,** *5* (5), 626.

(17) Yang, Z.; Liu, H.; Liu, D. Spatial regulation of synthetic and biological nanoparticles by DNA nanotechnology. *Npg Asia Materials* **2015,** *7*, e161.

(18) Thoniyot, P.; Tan, M. J.; Karim, A. A.; Young, D. J.; Loh, X. J. Nanoparticle-Hydrogel Composites: Concept, Design, and Applications of These Promising, Multi-Functional Materials. *Advanced science (Weinheim, Baden-Wurttemberg, Germany)* **2015,** *2* (1-2), 1400010.

(19) Fan, W. Z.; Tong, X.; Farnia, F.; Yu, B.; Zhao, Y. CO2-Responsive Polymer Single-Chain Nanoparticles and Self-Assembly for Gas-Tunable Nanoreactors. *Chem Mater* **2017,** *29* (13), 5693.

(20) Guo, Z. R.; Gu, H. J.; Ma, W.; Chen, Q.; He, Z. F.; Zhang, J. L.; Liu, Y. X.; Zheng, L. Z.; Feng, Y. J. CO2-switchable polymer-hybrid silver nanoparticles and their gas-tunable catalytic activity. *Rsc Adv* **2017,** *7* (78), 49777.

(21) Firestone, M. A.; Williams, D. E.; Seifert, S.; Csencsits, R. Nanoparticle arrays formed by spatial compartmentalization in a complex fluid. *Nano Lett* **2001,** *1* (3), 129.

(22) Wang, G.; Hoornweg, A.; Wolterbeek, H. T.; Franken, L. E.; Mendes, E.; Denkova, A. G. Enhanced Retention of Encapsulated Ions in Cross-Linked Polymersomes. *The Journal of Physical Chemistry B* **2015,** *119* (11), 4300.

(23) Matsumoto, M.; Terashima, T.; Matsumoto, K.; Takenaka, M.; Sawamoto, M. Compartmentalization Technologies via Self-Assembly and Cross-Linking of Amphiphilic Random Block Copolymers in Water. *J Am Chem Soc* **2017,** *139* (21), 7164.

(24) Grubjesic, S.; Ringstrand, B. S.; Jungjohann, K. L.; Brombosz, S. M.; Seifert, S.; Firestone, M. A. Cascade synthesis of a gold nanoparticle-network polymer composite. *Nanoscale* **2016,** *8* (5), 2601.

(25) Hayden, S. C.; Junghans, A.; Majewski, J.; Firestone, M. A. Reversible Lifting of Surface Supported Lipid Bilayers with a Membrane-Spanning Nonionic Triblock Copolymer. *Biomacromolecules* **2017,** *18* (4), 1097.

(26) Xu, M.; Liu, D. F.; Allen, H. C. Ethylenediamine at air/liquid and air/silica interfaces: Protonation versus hydrogen bonding investigated by sum frequency generation spectroscopy. *Environ Sci Technol* **2006,** *40* (5), 1566.

(27) Newman, J. D. S.; Blanchard, G. J. Formation of Gold Nanoparticles Using Amine Reducing Agents. *Langmuir* **2006,** *22* (13), 5882.

(28) Firestone, M. A.; Shank, M. L.; Sligar, S. G.; Bohn, P. W. Film Architecture in Biomolecular Assemblies. Effect of Linker on the Orientation of Genetically Engineered Surface-Bound Proteins. *J Am Chem Soc* **1996,** *118* (38), 9033.

(29) Grubjesic, S.; Lee, B.; Seifert, S.; Firestone, M. A. Preparation of a self-supporting cell architecture mimic by water channel confined photocrosslinking within a lamellar structured hydrogel. *Soft Matter* **2011,** *7* (20), 9695.

(30) Krishnamurty, S.; Stefanov, M.; Mineva, T.; Begu, S.; Devoisselle, J. M.; Goursot, A.; Zhu, R.; Salahub, D. R. Density Functional Theory-Based Conformational Analysis of a Phospholipid Molecule (Dimyristoyl Phosphatidylcholine). *J Phys Chem B* **2008,** *112* (42), 13433.

(31) Vyas, V.; Sancheti, P.; Karekar, P.; Shah, M.; Pore, Y. Physicochemical characterization of solid dispersion systems of tadalafil with poloxamer 407. *Acta. Pharm.* **2009,** *59*, 453.

(32) Stepniak, I.; Andrzejewska, E. *Electrochim. Acta* **2009,** (54), 5660.

(33) Rial, E.; Muga. *European journal of Biol* **1990,** *188*, 83.

(34) Merino, E. G.; Neves, P. D.; Fonseca, I. M.; Danede, F.; Idrissi, A.; Dias, C. J.; Dionisio, M.; Correia, N. T. Detection of two glass transitions on Triton X-100 under confinment. *J. Phys. Chem. C* **2013,** *117*, 21516.

(35) Xu, M.; Liu, D.; Allen, H. C. Ethylenediamine at Air/Liquid and Air/Silica Interfaces: Protonation Versus Hydrogen Bonding Investigated by Sum Frequency Generation Spectroscopy. *Environ Sci Technol* **2006,** *40* (5), 1566.

(36) Krishnan, K.; Plane, R. A. Raman and Infrared spectra of complexes of ethylenediamine with Zinc (II), Cadmium (II), adn Mercury (II). *Inorganic Chemistry* **1966,** *5* (5), 852.

(37) Lu, X.; Tan, C. Y.; Xu, J.; He, C. Thermal degradation of electrical conductivity of polyacrylic acid doped polyaniline: effect of molecular weight of the dopants. *Synthetic Metals* **2003,** *138* (3), 429.

(38) Mitsuda, K.; Kimura, H.; Murahashi, T. Evaporation and decomposition of Triton X-100 under various gases and temperatures. *J. Materials Sci.* **1989,** *24*, 413.

(39) Seyhan, M.; Kucharczyk, W.; Yarar, U. E.; Rickard, K.; Rende, D.; Baysal, N.; Bucak, S.; Ozisik, R. Interfacial surfactant competition and its impact on poly(ethylene oxide)/Au and poly(ethylene oxide)/Ag nanocomposite properties. *Nanotechnology, science and applications* **2017,** *10*, 69.

(40) Radi, B.; Wellard, R. M.; George, G. A. Controlled Poly(ethylene glycol) Network Structures through Silsesquioxane Cross-Links Formed by Sol−Gel Reactions. *Macromolecules* **2010,** *43* (23), 9957.

(41) Samanta, P.; Thangapandian, V.; Singh, S.; Srivastava, R.; Nandan, B.; Liu, C. L.; Chen, H. L. Crystallization behaviour of poly(ethylene oxide) under confinement in the electrospun nanofibers of polystyrene/poly(ethylene oxide) blends. *Soft Matter* **2016,** *12* (23), 5110.

(42) Beaudoin, E.; Phan, T. N. T.; Robinet, M.; Denoyel, R.; Davidson, P.; Bertin, D.; Bouchet, R. Effect of interfaces on the melting of PEO congined in triblock PS-b-PEO-PS copolymers. *Langmuir* **2013,** *29*, 10874.

(43) Firestone, M. A.; Wolf, A. C.; Seifert, S. Small-angle x-ray scattering study of the interaction of poly(ethylene oxide)-b-poly(propylene oxide)-b-poly(ethylene oxide) triblock copolymers with lipid bilayers. *Biomacromolecules* **2003,** *4* (6), 1539.

(44) Firestone, M. A.; Thiyagarajan, P.; Tiede, D. M. Structure and optical properties of a thermoresponsive polymer-grafted, lipid-based complex fluid. *Langmuir* **1998,** *14* (17), 4688.

(45) Lee, S.; Seifert, S.; Firestone, M. A. Multi-length scale evaluation of the temperature-tunable mechanical properties of a lyotropic mesophase. *Polym J* **2013,** *45* (2), 179.

(46) Lee, B.; Firestone, M. A. Electron density mapping of triblock copolymers associated with model biomembranes: Insights into conformational states and effect on bilayer structure. *Biomacromolecules* **2008,** *9* (6), 1541.

(47) Alverez-Lorenzo, C.; Rey-Rico, A.; Sosnik, A.; Taboada, P. Poloxamine-based nanomaterials for drug delilvery. *Frontiers in Bioscience* **2010,** *E2*, 424.

(48) Sandez-Macho, I.; Casas, M.; Lage, E. V.; Rial-Hermida, M. I.; Concheiro, A.; Alvarez-Lorenzo, C. Interaction of poloxamine block copolymers with lipid membranes: Role of copolymer structure and membrane cholesterol content. *Colloid Surface B* **2015,** *133*, 270.

(49) Zhang, F.; Stuhn, B. *Colloids Polymer Sci* **2007,** *285* (4), 371.

(50) Chu, C.-Y.; Chen, M.-H.; Wu, M.-L.; Chen, H.-L.; Chiu, Y.-T.; Chen, S.-M.; Huang, C.-H. Hierarchical Structure and Crystal Orientation in Poly(ethylene oxide)/Clay Nanocomposite Films. *Langmuir* **2014,** *30* (10), 2886.

(51) Yeh, S.-W.; Wei, K.-H.; Sun, Y.-S.; Jeng, U. S.; Liang, K. S. Morphological Transformation of PS-b-PEO Diblock Copolymer by Selectively Dispersed Colloidal CdS Quantum Dots. *Macromolecules* **2003,** *36* (21), 7903.

(52) Mao, W. T.; Cao, X.; Sheng, Q. Q.; Han, L.; Che, S. A. Silica Scaffold with Shifted "Plumber's Nightmare" Networks and their Interconversion into Diamond Networks. *Angew Chem Int Edit* **2017,** *56* (36), 10670.

(53) Mortensen, K.; Annaka, M. Structural Study of Four-Armed Amphiphilic Star-Block Copolymers: Pristine and End-Linked Tetronic T1307. *Acs Macro Letters* **2016,** *5* (2), 224.

(54) Ishoy, T.; Mortensen, K. Lamellar-to-cubic phase change in phospholipid bilayer systems incorporated with block copolymers: DMPC and PEO-PPO-PEO (P85). *Langmuir* **2005,** *21* (5), 1766.

(55) Angelova, A.; Ollivon, M.; Campitelli, A.; Bourgaux, C. Lipid cubic phases as stable nanochannel network structures for protein biochip development: X-ray diffraction study. *Langmuir* **2003,** *19* (17), 6928.

(56) Brown, M. F. Curvature Forces in Membrane Lipid-Protein Interactions. *Biochemistry-Us* **2012,** *51* (49), 9782.

(57) Kulkarni, C. V.; Wachter, W.; Iglesias-Salto, G.; Engelskirchen, S.; Ahualli, S. Monoolein: a magic lipid? *Phys Chem Chem Phys* **2011,** *13* (8), 3004.

(58) Singh, V.; Khullar, P.; Dave, P. N.; Kaura, A.; Bakshi, M. S.; Kaur, G. pH and thermo-responsive tetronic micelles for the synthesis of gold nanoparticles: effect of physiochemical aspects of tetronics. *Phys Chem Chem Phys* **2014**, 16 (10), 4728.

(59) Laible, P. D.; Kelley, R. F.; Wasielewski, M. R.; Firestone, M. A. Electron-transfer dynamics of photosynthetic reaction centers in thermoresponsive soft materials. *J Phys Chem B* **2005,** *109* (49), 23679.

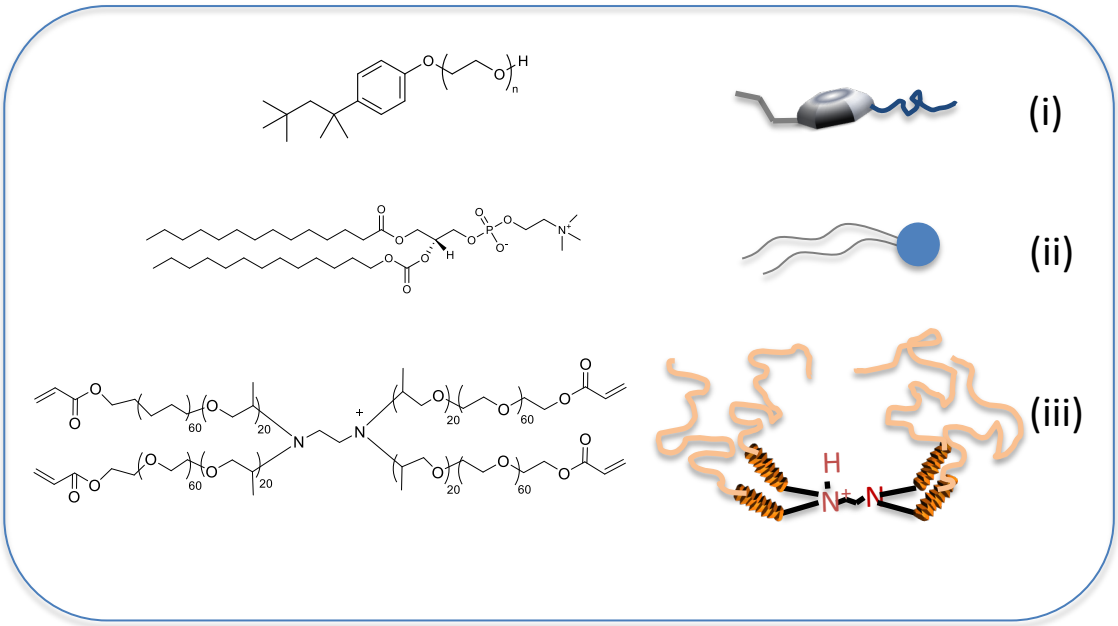

Fig.1

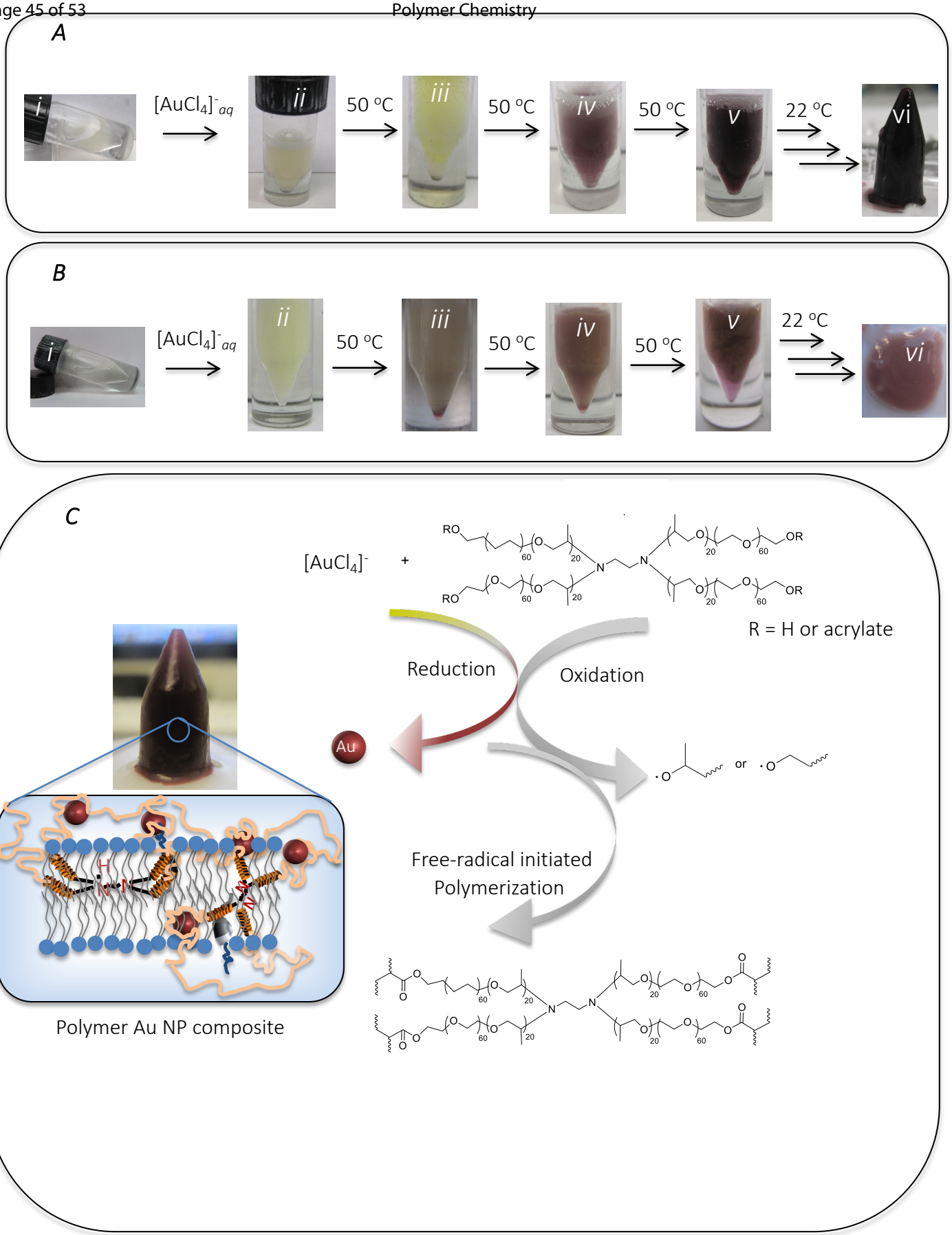
A
i
[AuCl4]-aq
ii
50 °C
iii
50 °C
iv
50 °C
v
22 °C
vi
B
i
[AuCl4]-aq
ii
50 °C
iii
50 °C
iv
50 °C
v
22 °C
vi
C
[AuCl4]-
+
RO
OR
R = H or acrylate
Reduction
Oxidation
Au
or
Free-radical initiated
Polymerization
Polymer Au NP composite

Fig.2

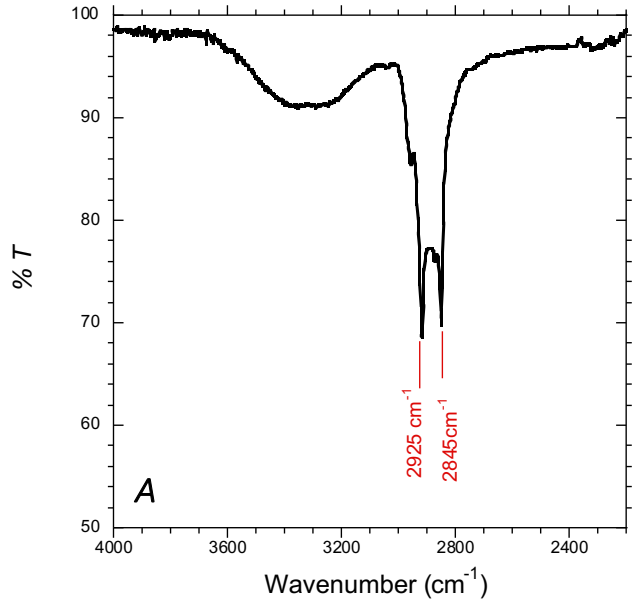
100
90
80
70
60
50
% T
2925 cm-1
2845cm-1
A
4000
3600
3200
2800
2400
Wavenumber (cm-1)

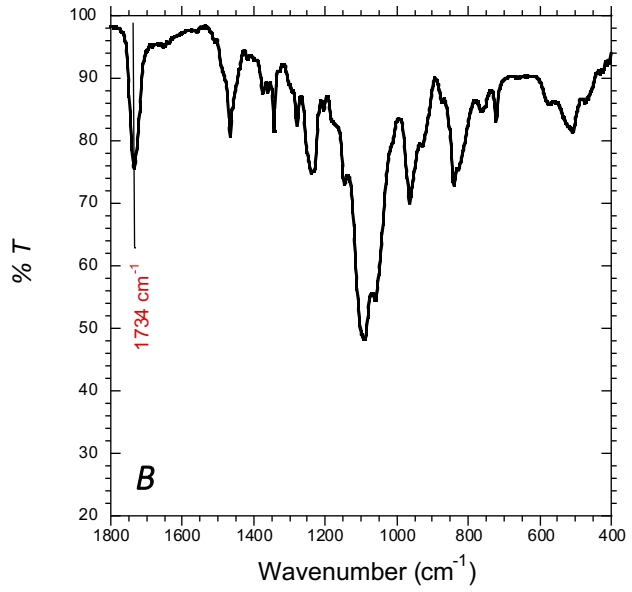
100
90
80
70
60
50
40
30
20
% T
1734 cm-1
B
1800
1600
1400
1200
1000
800
600
400
Wavenumber (cm-1)

Fig.3

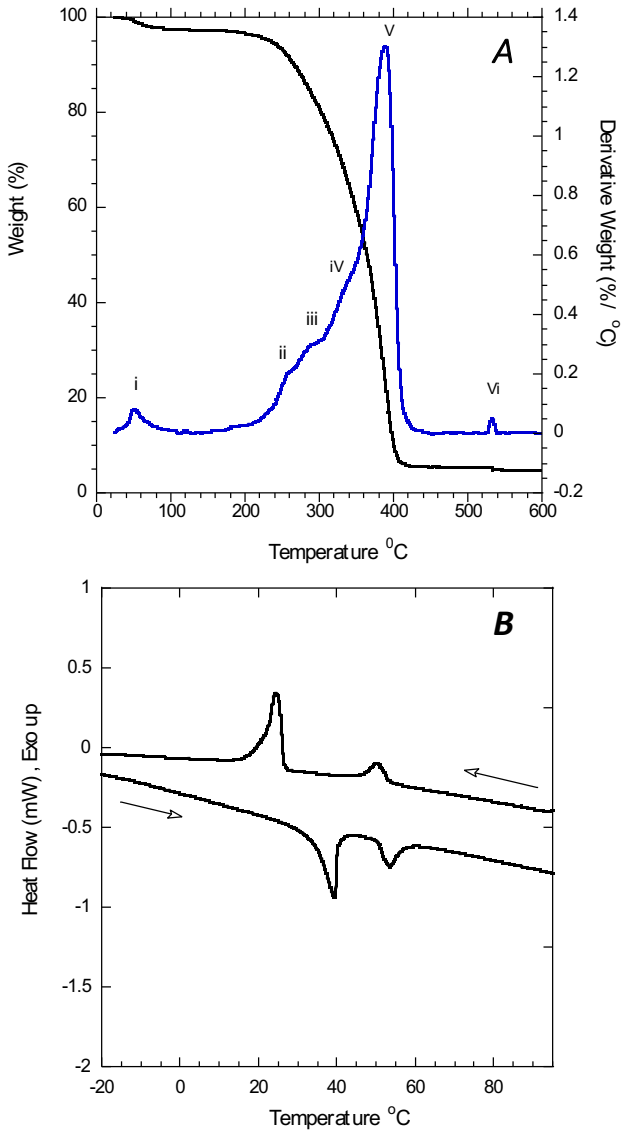
A
Weight (%)
Derivative Weight (%/ °C)
Temperature °C
i
ii
iii
iV
V
Vi
B
Heat Flow (mW), Exo up
Temperature °C

Fig. 4

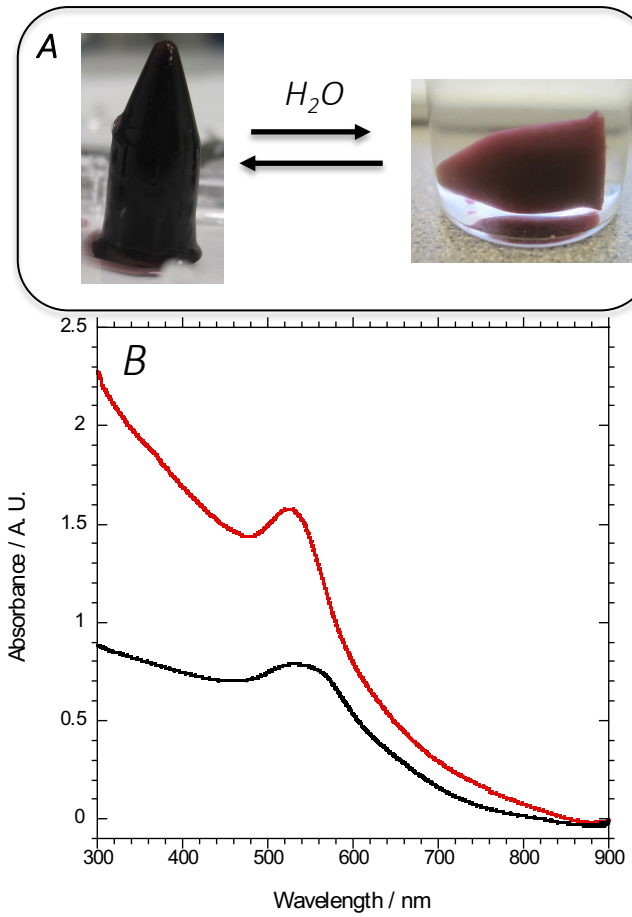
A
H_2O
B
Absorbance / A. U.
Wavelength / nm
2.5
2
1.5
1
0.5
0
300
400
500
600
700
800
900

Fig. 5

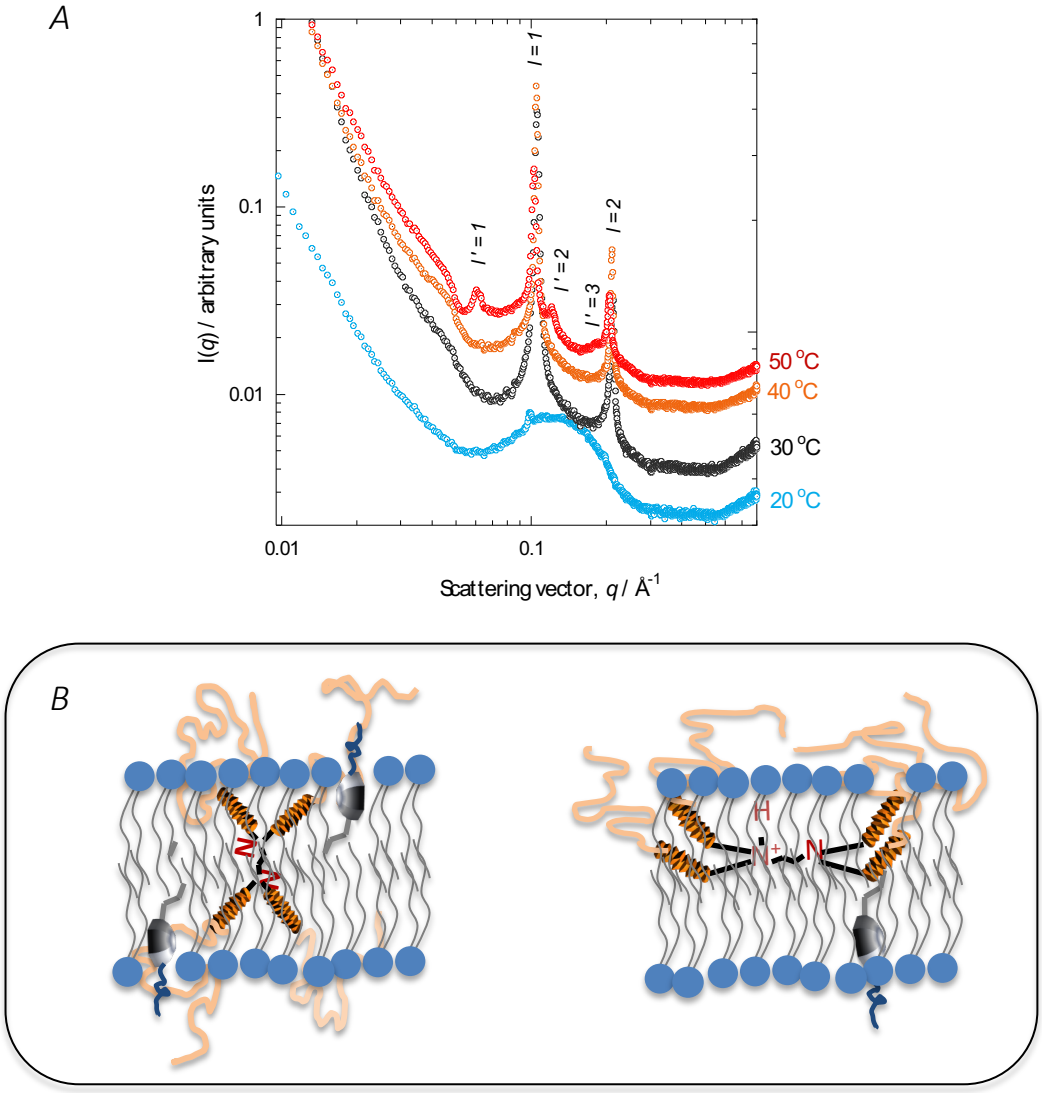
A
1
0.1
0.01
I(q) / arbitrary units
0.01
0.1
Scattering vector, q / Å-1
l = 1
l' = 1
l' = 2
l' = 3
l = 2
50 °C
40 °C
30 °C
20 °C
B
N
N
H
N+
N

Fig. 6

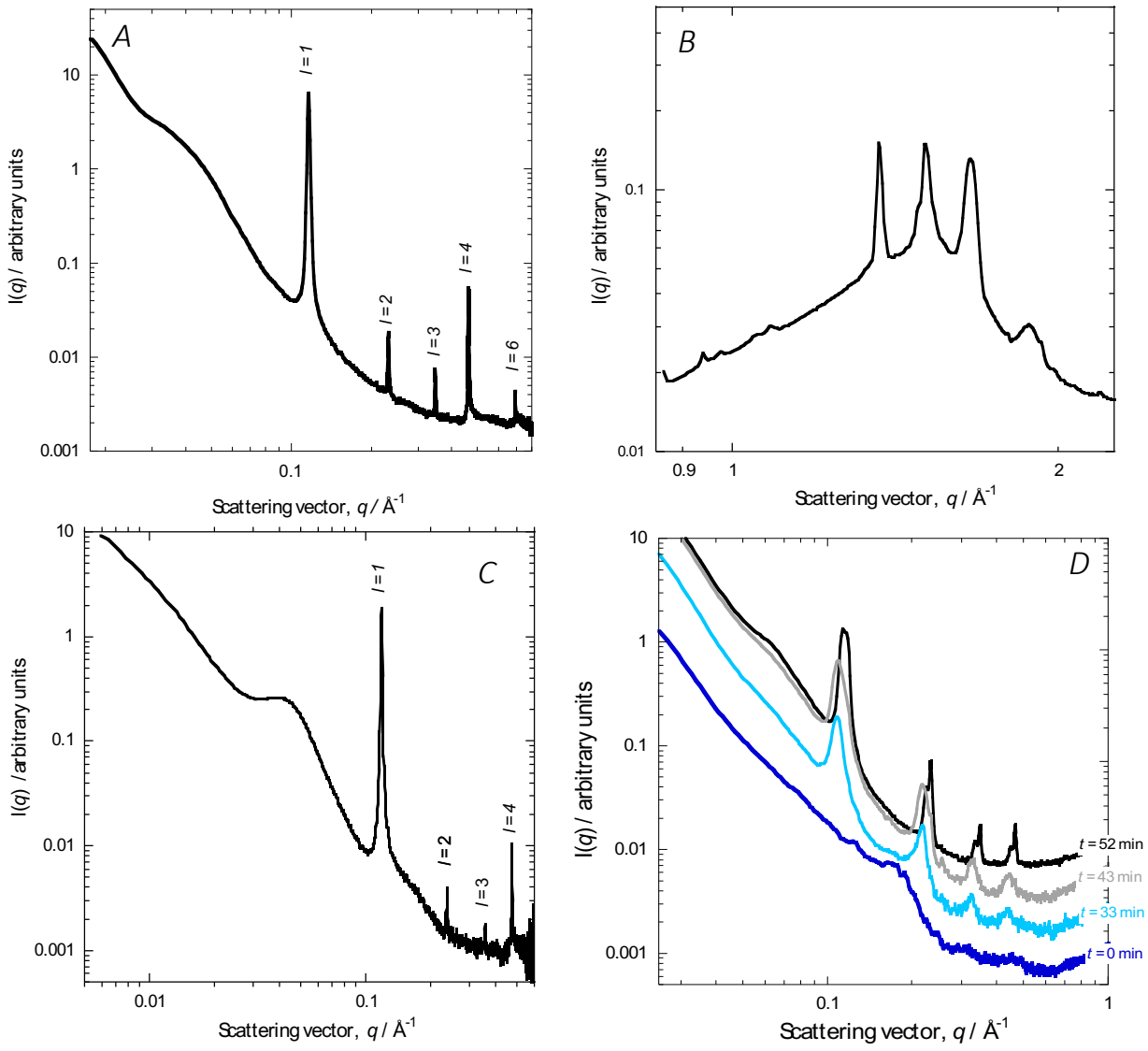
A
I = 1
I = 2
I = 3
I = 4
I = 6
I(q) / arbitrary units
Scattering vector, q / Å-1
B
I(q) / arbitrary units
Scattering vector, q / Å-1
C
I = 1
I = 2
I = 3
I = 4
I(q) /arbitrary units
Scattering vector, q / Å-1
D
t = 52 min
t = 43 min
t = 33 min
t = 0 min
I(q) / arbitrary units
Scattering vector, q / Å-1

Fig. 7

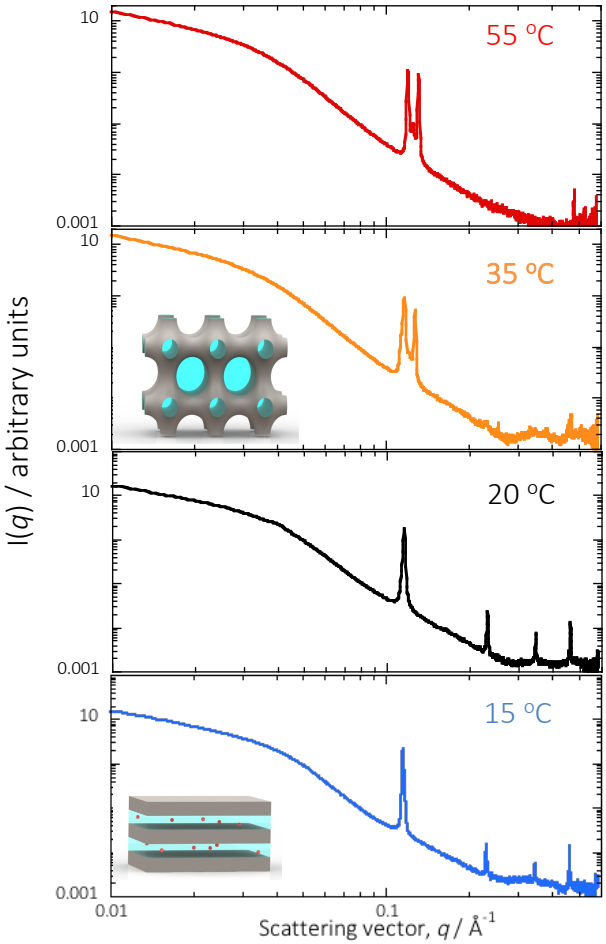
55 °C
35 °C
20 °C
15 °C
10
0.001
0.01
0.1
I(q) / arbitrary units
Scattering vector, q / Å-1

Fig. 8

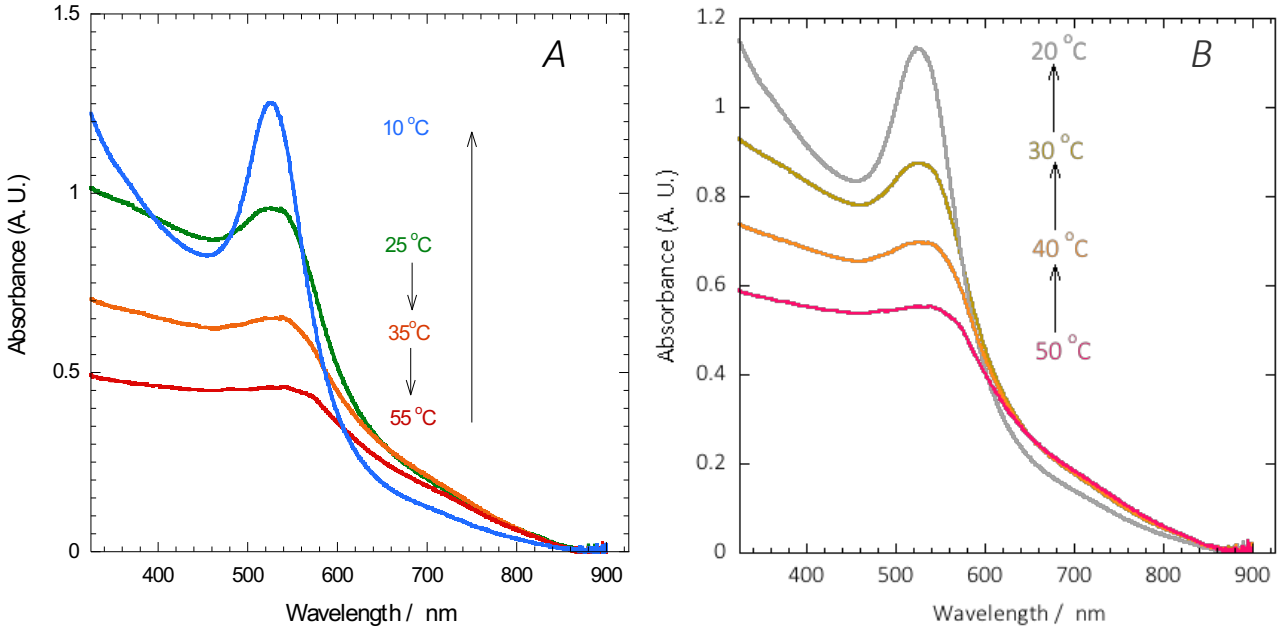
A
10 °C
25 °C
35 °C
55 °C
Absorbance (A. U.)
Wavelength / nm
B
20 °C
30 °C
40 °C
50 °C
Absorbance (A. U.)
Wavelength / nm

Fig. 9

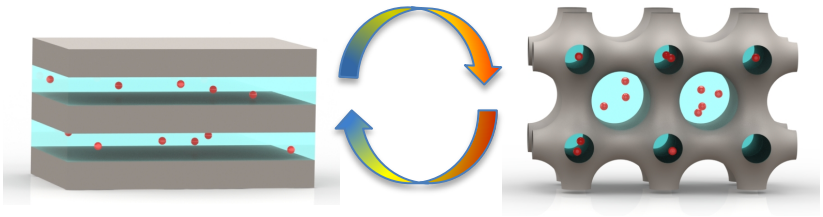

TOC